On-Chip Biosensing and Gas Sensing by Photonic Slot Waveguides: A Review

Francesco Dell'Olio, *Senior Member, IEEE*, and Carlos Angulo Barrios

***Abstract*—Photonic slot waveguides enhance light–matter interactions by confining the optical field in regions with a low refractive index, making them highly effective for detecting a wide range of biological and chemical analytes. This article reviews the application of photonic slot waveguides in biosensing and gas sensing, showcasing their ability to be integrated into on-chip platforms often intended for point-of-care testing with enhanced sensitivity and specificity. In biosensing, these waveguides are particularly suited for applications in medical diagnostics and environmental monitoring, allowing for the detection of biomarkers and other biological molecules with high sensitivity. For gas sensing, photonic slot waveguides have been employed effectively in the near-infrared and mid-infrared spectrum to detect various gases, including hazardous and greenhouse gases, which is crucial for both industrial safety and environmental protection. This review also explores the potential of these waveguides in noninvasive diagnostic methods, such as liquid biopsy, breath analysis, and breath biopsy, which offer new avenues for early disease detection and monitoring. By summarizing recent advancements and outlining future directions, this review underscores the transformative potential of photonic slot waveguides in advancing on-chip sensing technologies across multiple fields.**

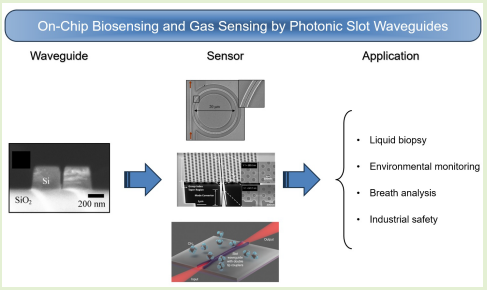

***Index Terms*— Biosensor, nanophotonics, sensor, silicon photonics, slot waveguide.**

I. Introduction

THE demand for rapid, low-cost, miniaturized, and accurate diagnostic and analytical tools has grown significantly in recent years, particularly in the healthcare sector where timely interventions can profoundly influence patient outcomes [1], [2]. Among the innovative diagnostic methodologies available, liquid biopsy [3], [4], [5] has emerged as a transformative approach, allowing for the detection, analysis, and monitoring of cancer through the analysis of body fluids such as blood or urine, rather than requiring tissue samples. This method analyzes various biological matrices including circulating tumor cells, cell-free nucleic acids, and exosomes. Liquid biopsy offers a non- or minimally invasive alternative to traditional methods, providing a more comprehensive view of tumor heterogeneity and enabling real-time monitoring of cancer progression. In contrast to liquid and tissue biopsies that necessitate the collection of blood or tissue samples, breath biopsy [6], [7] presents a completely noninvasive option for disease diagnosis. Breath analysis involves a highly sensitive analytical technique that is capable of accurately identifying a wide array of volatile organic compounds present in exhaled air, which can be indicative of various pathological conditions.

Currently, the vast majority of diagnostic methods often entail laborious laboratory procedures and specialized equipment, which present notable challenges in scenarios with limited resources or when immediate results are imperative. To address these challenges, point-of-care (PoC) and point-of-need (PoN) diagnostics have emerged as promising approaches [8], [9], [10]. These methodologies facilitate the direct delivery of diagnostic information to patients or healthcare providers, effectively bypassing the need for centralized laboratories and extensive processing times.

Photonic sensors are central to the advancements in PoC and PoN diagnostics and they leverage light for the detection of analytes and exhibit numerous advantages in biochemical, health, and environmental applications [11], [12]. These sensors enable multidimensional interrogation—intensity, wavelength, phase, and polarization—while remain-

Received 6 September 2024; revised 25 October 2024; accepted 28 October 2024. Date of publication 7 November 2024; date of current version 2 January 2025. The associate editor coordinating the review of this article and approving it for publication was Dr. Ing. Emiliano Schena. *(Corresponding authors: Francesco Dell'Olio; Carlos Angulo Barrios.)*

Francesco Dell'Olio is with the Micro Nano Sensor Group, Polytechnic University of Bari, 70125 Bari, Italy (e-mail: francesco.dellolio@poliba.it).

Carlos Angulo Barrios is with the Department of Photonics and Bioengineering, CEMDATIC, ETSI Telecomunicación, Universidad Politécnica de Madrid, 28040 Madrid, Spain (e-mail: carlos.angulo.barrios@upm.es).

Digital Object Identifier 10.1109/JSEN.2024.3490256

ing inherently immune to electromagnetic interference. The telecommunication industry's well-established technologies—such as various laser wavelengths, detector arrays, and advanced micro-/nanofabrication techniques—further support the deployment of these sensors. Importantly, the optical frequencies employed in VIS and near-IR match a wide array of physical properties inherent to biological materials, thereby enhancing the effectiveness of these sensing technologies.

Photonic biosensing can be achieved using two approaches: labeling-based detection, which involves attaching fluorescent or light-absorbing markers to target or recognition molecules; or label-free methods such as refractometry, Raman spectroscopy, or optical detection of mechanical deflections (e.g., cantilevers). Both detection techniques employ integrated microphotonic devices that rely on planar waveguides, providing notable benefits compared to conventional bulk optics and fiber optic-based biochemical sensors [13], [14], [15], [16]. Chip-scale planar waveguides utilize advanced technology that allows for efficient mass production using standard lithographic procedures. Additionally, this technology enables the integration of tiny device arrays on a single chip, which makes the simultaneous detection of many analytes possible. Additionally, the advancement of Si-based materials and CMOS technology has enabled the consolidation of sensors and electrical components onto a single chip, resulting in improved sensor capabilities and reduced size.

Within the realm of integrated microphotonics for biochemical sensors, traditional strip and rib waveguides, which rely on total internal reflection in a high-index material surrounded by a low-index material, are still commonly used. However, new designs such as hollow-core waveguides have also been investigated [17], [18]. These waveguides, which direct light in materials with a low refractive index, are especially important for biological sensing because they can hold fluids in their hollow core. However, they are highly dependent on the wavelength of light due to optical interference.

The slot waveguide is a groundbreaking advancement in waveguide design that fundamentally transforms the way light is guided and confined [19], [20]. This waveguiding structure allows for the precise confinement of light within a nanoscale region of the space with a low refractive index, achieved through total internal reflection. This is a unique capacity that is not achievable with traditional waveguides. Slot waveguides are particularly advantageous for biosensing applications. By utilizing the slot as a sensing region, it enables improved interaction between light and analytes, resulting in increased sensitivity compared to conventional waveguides [13]. Furthermore, slot waveguides are immune to interference effects and exhibit negligible sensitivity to changes in wavelength due to their dependence on total internal reflection. Due to the very high index contrast allowed by that substrate, most dielectric slot waveguides have been manufactured in silicon-on-insulator (SOI) technology but other material systems, such as Si_3N_4/SiO_2 [21], SU8/SiO_2 [22], electrooptic polymer/TiO_2 [23], [24], and III–V semiconductors [25], have also been proposed in this context. At the state-of-the-art, silicon and silicon nitride remain the standard for dielectric slot waveguides. The above-mentioned alternative material platforms are primarily intended for nonlinear applications, but they generally do not present significant advantages over conventional platforms in terms of sensitivity in biosensing contexts. With the aim of downscaling dielectric slot waveguides, plasmonic slot waveguides have been experimentally demonstrated and studied [26], [27], [28].

The recent advancement of microphotonic technologies has led to significant impacts in the fields of biosensing and gas sensing through the development of chip-scale sensors. These sensors are increasingly essential in various application scenarios, including environmental monitoring and sensor-based internet-of-things (IoT) systems. The overarching aim in these domains is to develop sensing platforms that are cost-effective, easy to interrogate, as well as being capable of detecting a broad range of biomarkers and chemical species with high selectivity and sensitivity. Achieving these goals via integrated microphotonics necessitates optimized waveguide configurations that maximize light–matter interaction, a challenge that slot waveguides effectively address.

This article provides a comprehensive review of the state of the art in photonic slot waveguides, emphasizing their role in refractive index-based gas sensing and biosensing applications. By elucidating the fundamental principles of slot waveguides and highlighting their unique features such as high optical confinement and enhanced sensitivity, this review aims to showcase the transformative potential of these technologies in advancing the field of biosensing and gas sensing.

Major milestones and selected key directions for the research on photonic slot waveguides for biosensing and gas sensing are summarized in Fig. 1.

II. Fundamentals

The typical configuration of a slot waveguide in the SOI (Si/SiO_2) material system is shown in Fig. 2(a). It consists of two Si-wires whose geometrical dimensions are h (height) and w (width). The wires or rails are separated by a gap or slot of width g. The wire height typically ranges from 220 to 300 nm, which is the usual thickness of the silicon top layer in SOI wafers for photonic applications. The g value is approximately 50–100 nm, while w is usually in the range of 200–300 nm. In biosensing and gas sensing applications, the waveguide cladding, which commonly fills the slot, is either a liquid solution in which the analytes are dispersed or a gas mixture. In other applications, a variety of low-index materials, including air, silicon oxide, and polymers [e.g., poly(methyl methacrylate) (PMMA)], are utilized. In addition to Si, other high-index materials, such as silicon nitride or titanium dioxide, can be used for the wires.

The parameter quantifying the optical intensity within the gap between the wires is the confinement factor Γ, which is defined as

$$\Gamma = \iint_{\Sigma} |\mathbf{E}(x, y)|^2 dx dy \Big/ \iint_{\infty} |\mathbf{E}(x, y)|^2 dx dy \qquad (1)$$

where $\mathbf{E}$ is the electric field and Σ is the slot region between the wires.

Electromagnetic propagation in slot waveguides is due to the total internal reflection. The physical origin of the light

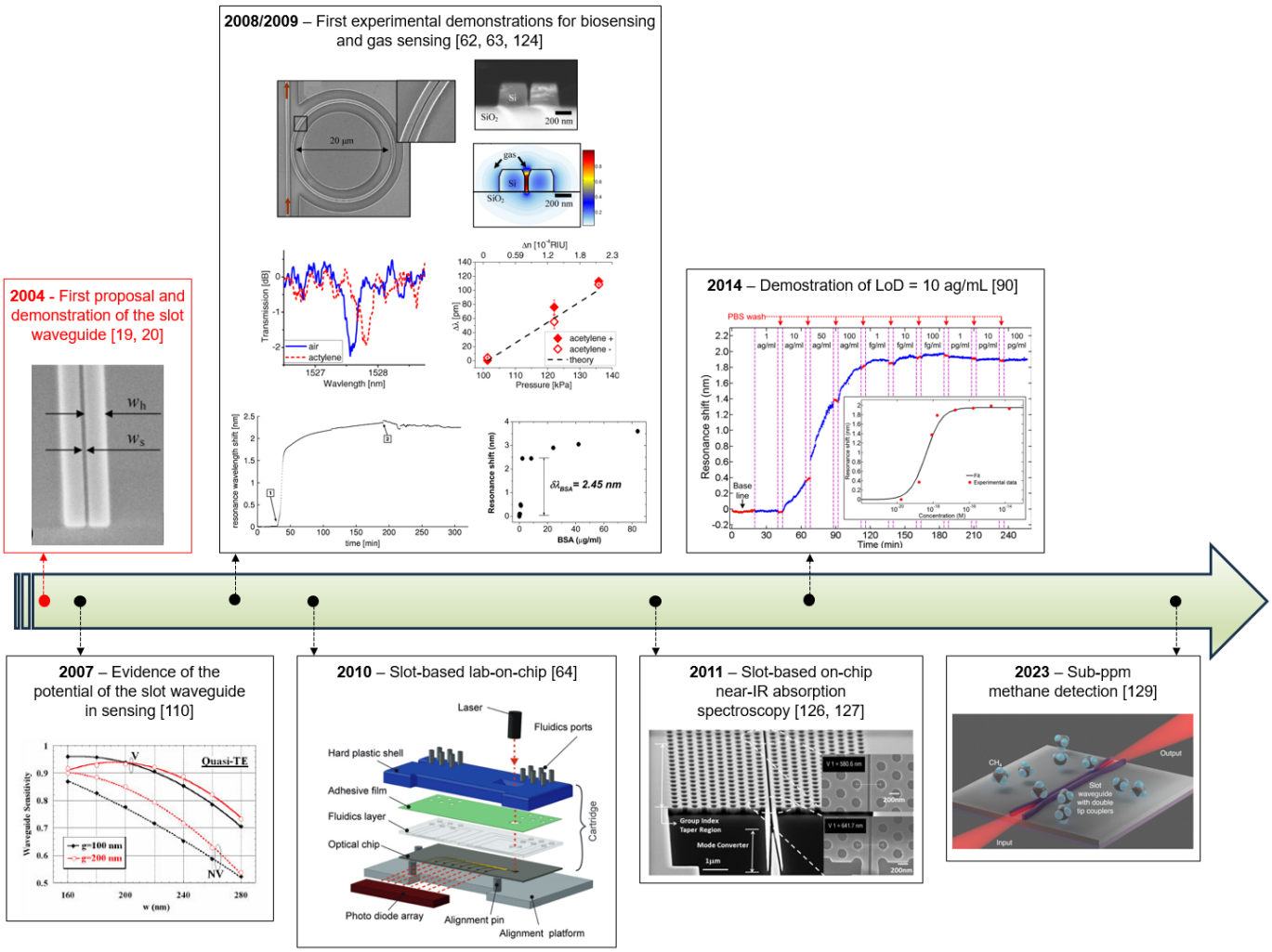

Fig. 1. Major milestones and achievements in the field of photonic slot waveguides for biosensing and gas sensing. Reprinted with permission from [19], [20], [62], [63], [64], [90], [110], [124], [126], [127], and [129].

confinement within the slot is the continuity of the normal component D_x of the electric displacement field **D** across the vertical Si/cladding interfaces. Since **E** is equal to $\varepsilon_0\, n^2\, \mathbf{D}$ (n is the refractive index and ε_0 is the vacuum permittivity), the continuity condition on **D** implies a discontinuity in the normal component (E_x) of **E** due to the discontinuity in n across the vertical Si/cladding interfaces. The two discontinuities in E_x at the two slot vertical boundaries, typically separated by a distance $\leq$100 nm, induce the light confinement in the gap between the wires.

The slot waveguide is capable of supporting the fundamental quasi-TE mode, which is well confined within the slot (with confinement factors exceeding 50%), and the fundamental quasi-TM mode, which exhibits a confinement factor in the slot of less than 5%.

The effective index (n_{eff}) and phase velocity of the quasi-TE mode, which is the slot mode, are strongly influenced by the refractive index n_S of the low-index medium filling the slot. This key feature enables nearly all practical applications of slot waveguides. The sensitivity of n_{eff} to small changes of n_S can be derived according to the variational theorem for dielectric waveguides [29], and is given by

$$S = \frac{\partial n_{eff}}{\partial n_S} = 2\, n_S^0 \Gamma \Pi \tag{2}$$

where

$$\Pi = \iint_{\infty} \left(|\mathbf{E}|^2 / Z_0 P_z\right) dx dy. \tag{3}$$

Z_0 is the free space impedance, n_S^0 is the unperturbed value of n_S, and P_z is the z-component of the Poynting vector **P** (z is the propagation direction).

As shown in (2), the sensitivity of n_{eff} to refractive index change within the slot is proportional to Γ, which is a key parameter influencing the performance of nearly all devices based on slot waveguides.

To illustrate the properties of modes supported by slot waveguides, we assume $h = 260$ nm, $w = 220$ nm, and $g = 100$ nm for the waveguide in Fig. 2(a). We assume the operating wavelength as equal to 1.55 μm. Simulations performed using the 3-D finite element method (FEM) show that, for the quasi-TE mode (effective index = 1.450), the

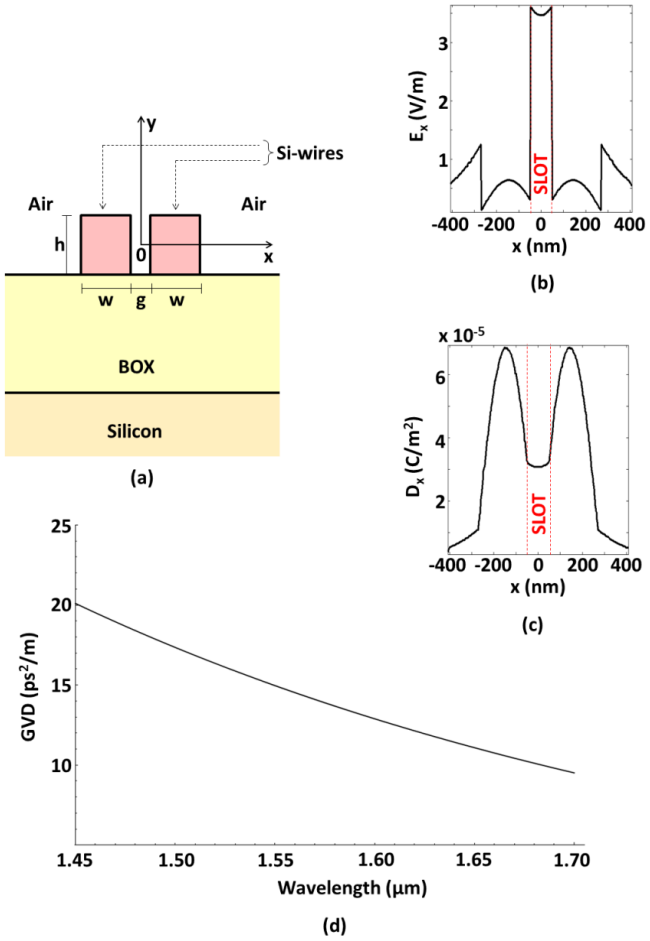

Fig. 2. (a) Cross section of the typical slot waveguide consisting of two Si rails separated by an air slot on a buried silicon oxide (BOX) layer. (b) Dependence of E_x and (c) D_x on x, $y = 0$, for 1.55 μm wavelength. (d) GVD dependence on the wavelength around 1.55 μm.

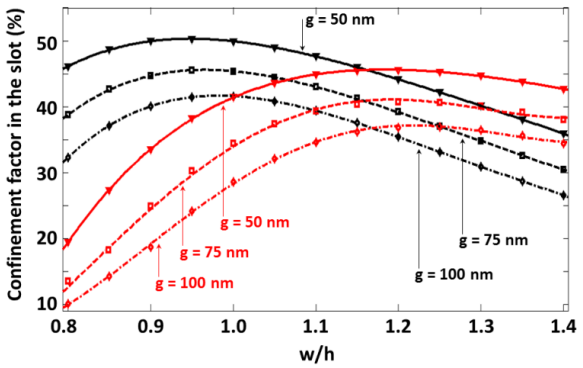

Fig. 3. Dependence of the confinement factor in the slot on the ratio w/h for several values of g ranging from 50 to 100 nm. Two values of the thickness of the silicon layer were considered: $h = 220$ nm (red curves) and 260 nm (black curves).

confinement factor in the slot is close to 40%, while it is <3% for the quasi-TM mode (effective index = 1.632). Assuming that the optical power carried out by the quasi-TE mode is 1 mW, the dependence of E_x (major component of **E**, for the TE mode) and D_x on x is plotted in Fig. 2(b) and (c). D_x is the **D** component normal to the Si/air vertical interfaces and thus it is continuous. Due to the refractive index discontinuity at the Si/air vertical interfaces, E_x is discontinuous at such interfaces and reaches its maximum within the slot. The TE mode group index is 2.45, at the operating wavelength.

The group velocity dispersion (GVD) of the considered Si slot waveguide is shown in Fig. 2(d), expressed in terms of $\beta_2 = \partial^2\beta/\partial\omega^2$ (ω is the angular frequency and β is the propagation constant). FEM-based calculations take into account the material dispersion through the Sellmeier equations for Si and SiO_2.

The GVD decreases from 20 ps^2/m to 9.5 ps^2/m when the wavelength increases from 1.45 to 1.70 μm. The dispersion is always normal (>0) across the wavelength range of 1.45–1.70 μm, and it equals 15 ps^2/m at the operating wavelength. As demonstrated in [30] and [31], the GVD of slot waveguides can be tailored by appropriately designing their geometrical dimensions. A zero-dispersion wavelength close to 1.55 μm can be obtained.

The confinement factor Γ of the slot mode depends on both the ratio w/h and the gap width, for a given h value. For the Si slot waveguide depicted in Fig. 2(a), the dependence of Γ on w/h is shown in Fig. 3. Two h values have been considered: $h = 220$ nm (red curves) and 260 nm (black curves). The slot width g is equal to 50, 75, and 100 nm. The confinement increases as the ratio w/h increases up to a maximum. After reaching the maximum value, Γ decreases as w/h increases. The value of w/h that maximizes the confinement is approximately 1.20 and 0.95 for $h = 220$ and 260 nm, respectively. The g reduction induces an increase in the confinement, and the maximum achievable value of Γ increases as h increases. The maximum confinement (>50%) is obtained for $h = 260$, $w = 247$, and $g = 50$ nm,

Although the configuration depicted in Fig. 2(a), known as a vertical slot waveguide, has been demonstrated to be highly versatile in numerous application fields, several alternative configurations have been proposed over the last few years.

Strip-loaded slot waveguides [Fig. 4(a)] including a wide strip-loading region with a thickness d of some tens of nanometers, where silicon is partially etched, are used in the context of high-speed modulators manufactured by filling the slot with an electrooptic polymer [32]. A similar waveguide configuration, in which the high-index medium, silicon-rich silicon nitride, is partially etched also within the slot, has been employed in a chemical sensor [33]. The same waveguide configuration has been used to demonstrate a polymer slot waveguide with a propagation loss of 20 dB/cm operating at visible wavelengths [34].

Asymmetric slot waveguides [Fig. 4(b)], in which the widths of the two wires (w_1 and w_2) are not equal and so the slot is not located at the center of the waveguide, have been proposed to design ultra-sharp 90° bends (radius = 1 μm) having a loss <2 dB [35]. Their potential for enhancing GVD tailoring has also been investigated [36].

Horizontal slot waveguides [Fig. 4(c)] [37], [38], [39], [40] consist of a nanolayer of a low-index material, such as silicon oxide, with a thickness g, sandwiched between two high-index

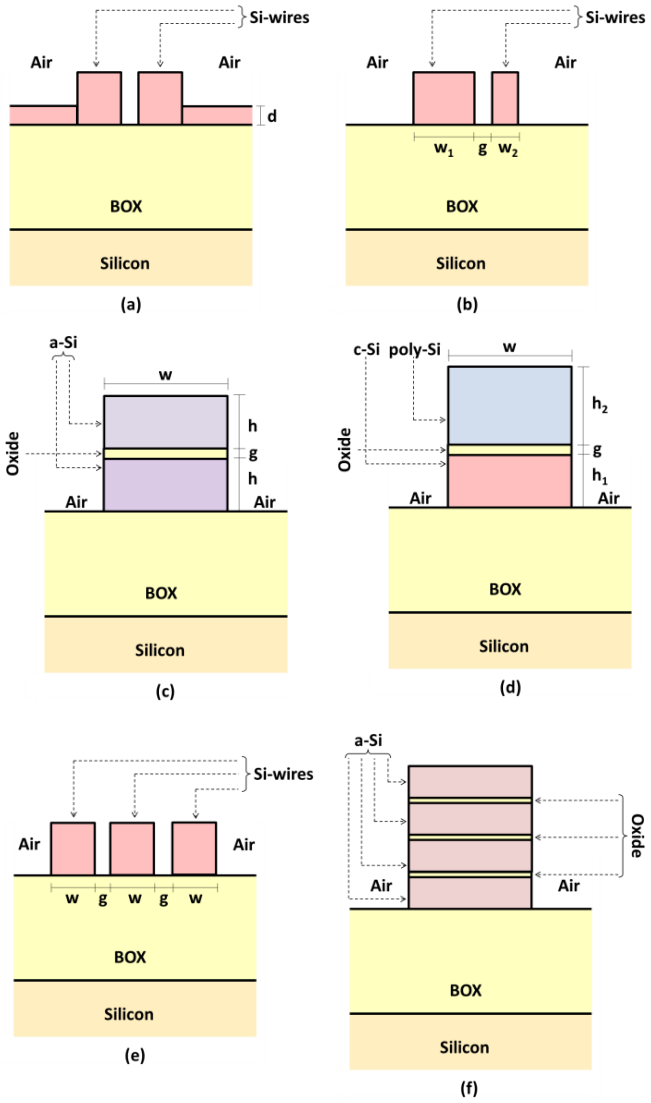

Fig. 4. Alternative configurations of slot waveguides: cross sections. (a) Strip-loaded. (b) Asymmetric. (c) Horizontal symmetrical. (d) Horizontal asymmetrical. (e) Multiple slots (vertical). (f) Multiple slots (horizontal).

layers with a thickness h. This configuration typically exhibits a lower loss than its vertical counterpart due to the low roughness (<1 nm) of the horizontal boundaries of the slot, where the **E**-field intensity is maximum. In this case, high **E**-field confinement in the slot is found for the quasi-TM mode, and the slot thickness can be reduced down to a few tens of nm. The high-index material used in these waveguides is typically amorphous silicon (a-Si) or polysilicon (poly-Si), which unfortunately have a higher bulk optical absorption than crystalline silicon (c-Si). The waveguide width w is in the range of 500–700 nm. Asymmetric horizontal slot waveguides have also been demonstrated [Fig. 4(d)], in which the high-index layers with different thicknesses (h_1 and h_2) are made of distinct materials (e.g., poly-Si and c-Si).

Multiple-slot (multi-slot) waveguides [22], [37], which include several slots, have been demonstrated to enhance the optical confinement in the slot regions. These waveguides can

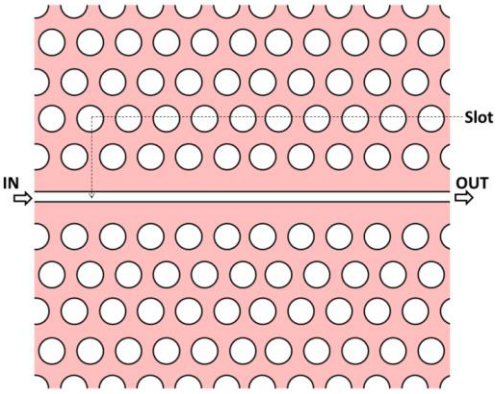

Fig. 5. Slotted photonic crystal slab waveguide.

be implemented in either a vertical configuration [Fig. 4(e)] or a horizontal configuration [Fig. 4(f)]. The incorporation of multiple slots can enhance the confinement factor in low-index regions. However, this may lead to multimode configurations. To achieve single-mode operation, meticulous waveguide design is essential [41]. Alternatively, techniques to eliminate higher-order modes can be employed. For instance, higher-order modes may not persist through waveguide bends due to elevated propagation losses [42].

In all mentioned alternative configurations, the waveguide cladding can be air, a gas mixture, an aqueous solution, or another low-index material such as SiO_2 or a polymer.

The group index of slot modes is usually close to the effective index, exhibiting a value of a few units. In contrast, line defects in 2-D PhC slabs allow the propagation of optical beams with a very high group index, thereby enhancing the light–matter interaction. Slotted photonic crystal waveguides (Fig. 5) [43], which feature a narrow slot within the line defect of a 2-D PhC slab, have been proposed and demonstrated aiming at merging the advantages of PhCs and slot waveguides. Group index values >100 have been experimentally proved using a slotted 2-D PhC slab (lattice constant = 490 nm, hole radius = 140 nm) with a 100-nm width slot, fabricated on an SOI wafer [44]. The propagation loss of slotted photonic crystal waveguides was experimentally investigated in [45]. The reported results show that a propagation loss <11 dB/cm can be achieved with a slot width of 135 nm.

Since 2005, when the first plasmonic slot waveguides consisting of a narrow slot in a thin metal film were proposed/demonstrated [46], [47], [48], the research effort on this topic has grown constantly and has led to the proposal of new configurations. The guiding structure in Fig. 6 includes two vertical metal/dielectric interfaces at which the real part of the dielectric constant ε undergoes a change of sign (in the near-infrared region, the real part of ε is negative for a metal and positive for a dielectric). This strong discontinuity in the real part of ε induces a discontinuity in the electric field **E**. The two closely spaced **E** discontinuities across the two vertical metal/dielectric interfaces are responsible for the light confinement in the slot.

The confinement factor Γ of the slot mode supported by the plasmonic waveguide in Fig. 6 increases as the slot width g

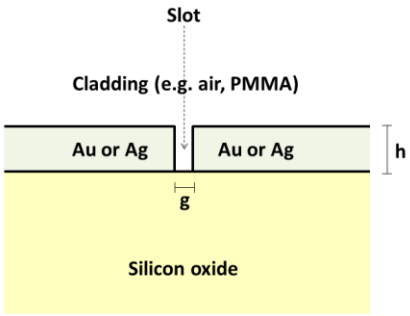

Fig. 6. Plasmonic slot waveguide: typical cross section.

decreases, achieving values close to 80% for $g = 20$ nm and $h = 200$ nm (we assume an air-filled slot in a gold film deposited on a SiO_2 layer and an operating wavelength of 1550 nm). Unfortunately, as g decreases, the waveguide propagation loss increases. Thus, the slot width should be optimized in order to achieve a suitable trade-off between high confinement and low propagation loss.

Electron beam lithography (ELB) followed by inductively coupled plasma (ICP) reactive ion etching (RIE) is the most typical approach for the fabrication of slot waveguides. For applications other than biosensing and gas sensing, a low-index top cladding layer cladding is commonly deposited by plasma-enhanced chemical vapor deposition (CVD) after the etching process.

In the last few years, deep UV lithography at 193 and 248 nm has been demonstrated as an efficient tool for slot waveguide fabrication [49], [50].

For horizontal slot waveguides, CVD is usually employed for the deposition of a multilayer structure, which is then patterned by either EBL or deep UV lithography followed by etching.

Additionally, nanoimprinting technology has been employed to fabricate a polymer slot waveguide for sensing applications. The silicon mold was fabricated by EBL and ICP-RIE and was used to manufacture a polymer-on-glass mold for the waveguide fabrication through nanoimprinting and UV curing [51].

Plasmonic slot waveguides have been manufactured by metal deposition by sputtering or evaporation, EBL, and ion milling or focused ion beam for the patterning of the guiding structure [52], [53].

Dielectric vertical slot waveguides are typically preferred for biosensing and gas sensing applications over a horizontal configuration, as the fabrication of a hollow slot sensing region is a more straightforward process. Propagation loss of dielectric vertical slot waveguides is dominated by scattering loss due to surface roughness at the vertical boundaries of the slot. The geometrical dimensions of the two wires, refractive index of the medium filling the slot, and the roughness standard deviation/correlation length are the main technological parameters influencing the propagation loss. An increase in wire width and a decrease in both wire height and roughness standard deviation have a beneficial effect on the propagation loss. The coating of vertical slot waveguides with a thin film of titanium or aluminum oxide via atomic layer deposition has been shown to reduce the propagation loss [54], [55]. The smoothing of vertical sidewalls through a few cycles of standard RCA clean [56] has allowed the demonstration of Si slot waveguides with propagation loss <5 dB/cm. Scattering loss is negligible in horizontal slot waveguides, in which propagation loss is primarily attributed to material absorption, with values as low as 1.8 dB/cm [57].

In biosensing applications, the wavelength-dependent light absorption of aqueous solutions also affects the propagation loss of slot waveguides. The water absorption is negligible at visible wavelengths and relatively low in the short-wave near-infrared region between 700 and 900 nm (water absorption coefficient of the order of 0.1 dB/cm). However, it increases 2–3 orders of magnitude at the typical telecom wavelengths, reaching values of several tens of dB/cm [58].

Due to the high optical absorption of metals in the near infrared, plasmonic slot waveguides exhibit a propagation loss that is three or four orders of magnitude greater than that of their dielectric counterparts. This critical aspect limits the length of devices based on those waveguides to a few micrometers.

III. Biosensing

Since their invention, slot waveguides have been widely used to develop and demonstrate integrated microphotonic transducers for biosensors. In this application, slot waveguides have been shown to outperform conventional strip waveguides. This superior performance arises from its remarkable ability to enhance the optical field in the low refractive-index slot region, which contains the sensitive element and is filled with the fluidic liquid sample of interest.

Table I summarizes some of the key achievements using slot-waveguide refractometric transducers and biosensors reported in the literature. Most devices are based on Si-based materials (Si, SiO_2, Si_3N_4), which is a consequence of the advantages of CMOS processing. This technology enables the implementation of vertical and horizontal slot waveguides in guided-wave interferometric configurations (e.g., Mach–Zehnder and Young interferometers) and optical cavities (e.g., ring and Fabry-Perot resonators). Two sensitivity values are typically provided for refractometric sensors: bulk or homogenous sensitivity, which refers to the device's ability to detect refractive index changes in the bulk-sensitive region surrounding the waveguide; and surface sensitivity, which is the sensitivity to local refractive index changes at the sensor surface. Another important parameter is the limit of detection (LoD), which is the minimum amount of analyte or refractive index change that can be reliably detected. LoD is typically defined as LoD = R/S, where S is the sensitivity and R is the sensor resolution. The sensor resolution is commonly considered to be equal to 3σ, where σ is the standard deviation of the total system noise.

The field of biosensing applications of slot waveguides was reviewed for the first time in 2009 [59]. Since then, there has been a continuous increase in both theoretical proposals and experimental demonstrations of slot-waveguide biosensors. This scientific production has been made possible by innovations and breakthroughs in the field, such as the

TABLE I
SLOT-WAVEGUIDE-BASED BIOSENSORS AND REFRACTOMETRIC TRANSDUCERS. ONLY THOSE WITH EXPERIMENTAL RESULTS ARE INCLUDED

Year Authors [Ref.]	Material system	Configuration	Bulk Sensitivity	Receptor/ Analyte	LoD
2007 Barrios et al. [61]	Si_3N_4/SiO_2	Vertical SW / Ring resonator	212 nm/RIU		$2\cdot10^{-4}$ RIU
2008 Barrios et al. [62]	Si_3N_4/SiO_2	Vertical SW / Ring resonator		Anti-BSA / BSA	16 pg/mm^2
2009 Di Falco et al. [83]	Si/SiO_2	Vertical SW / Photonic crystal cavity	1538 nm/RIU		$7.8\cdot10^{-6}$ RIU
2009 Sun et al. [22]	$SU8/SiO_2$	Vertical multiple SW / Ring resonator	244 nm/RIU	Biotin / BSA	
2009 Claes et al. [63]	Si/SiO_2	Vertical SW / Ring resonator	298 nm/RIU	Biotin / Avidin	$4.2\cdot10^{-5}$ RIU
2010 Carlborg et al. [64]	Si_3N_4/SiO_2	Vertical SW / Ring resonator	246 nm/RIU	Anti-BSA	0.9 pg/mm^2 $5\cdot10^{-6}$ RIU
2010 Jágerská et al. [84]	Si/SiO_2	Vertical SW / Photonic crystal cavity	510 nm/RIU		10^{-5} RIU
2010 Wang et al. [88]	InGaAsP	Vertical SW / Photonic crystal cavity	900 nm/RIU		
2011 Scullion et al. [85]	Si/SiO_2	Vertical SW / Photonic crystal cavity	500 nm/RIU	Biotin / Avidin	1 µg/mL 60 pg/mm^2
2012 Jugessur et al. [99]	Si/SiO_2	Vertical SW / Bragg grating	~500 nm/RIU		
2012 Tu et al. [33]	Si_3N_4/SiO_2	Vertical SW / MZI	1730 (2π)/RIU		1.3 pg/mm^2 $1.29\cdot10^{-5}$ RIU
2013 Wang et al. [100]	Si/SiO_2	Vertical SW / Bragg grating	340 nm/RIU	Anti-streptavidin / Streptavidin / Biotin-BSA	$3\cdot10^{-4}$ RIU
2013 Mirsadegui et al. [86]	Si/SiO_2	Vertical SW / Photonic crystal cavity	370 nm/RIU		$2.3\cdot10^{-5}$ RIU
2013 Liu et al. [76]	Si_3N_4/SiO_2	Vertical SW / MZI	1864π/RIU	Biotin / Streptavidin Methylated DNA	$5.4\cdot10^{-6}$ RIU 1 pg/mL (streptavidin)
2013 Xu et al. [89]	Si/SiO_2	Vertical SW / Photonic crystal cavity	410 nm/RIU		
2014 Hiltunen et al. [81]	Polymeric materials	Vertical SW / Young interferometer			$6.4\cdot10^{-6}$ RIU
2014 Yang et al. [90]	Si/SiO_2	Vertical multiple SW / Photonic crystal cavity	451 nm/RIU	Biotin / Streptavidin	10 ag/mL
2015 Sun et al. [77]	$Ag/Si/SiO_2$	Vertical SW / MZI	1061 nm/RIU		
2016 Taniguchi et al. [65]	Si_3N_4/SiO_2	Vertical SW / Ring resonator	141 nm/RIU	Biotin/ Streptavidin Anti-PSA / PSA	50 ng/mL (PSA)
2017 Steglich et al. [66]	Si/SiO_2	Vertical SW / Ring resonator	106.29 nm/RIU		
2018 Luan et al. [73]	Si/SiO_2	Vertical multibox SW / Ring resonator	580 nm/RIU	Anti-Streptavidin / Streptavidin / Biotin-BSA	$1.02\cdot10^{-3}$ RIU $3.13\cdot10^{-1}$ nm
2019 Xu et al. [94]	Si/SiO_2	Vertical multiple SW / Photonic crystal cavity	586 nm/RIU		
2019 Luan et al. [101]	Si/SiO_2	Vertical multibox SW / Bragg grating	579.2 nm/RIU	Biotin-BSA / Streptavidin / Biotin	~20 nM (biotin)
2020 Heinsalu et al. [102]	Si/SiO_2	Vertical multiple SW / Bragg grating	730 nm/RIU		

SW: Slot waveguide. MZI: Mach-Zehnder interferometer. RIU: Refractive index unit. LoD: limit of detection. BSA: Bovine serum albumin. PSA: Prostate-specific antigen.

investigation of polymer-based configurations, the analysis and demonstration of novel slot waveguide and transducer designs, the development of multislot waveguiding devices, and the introduction of slot-waveguide sensing configurations based on photonic crystals (1-D and 2-D) and subwavelength grating (SWG) structures.

This section provides an overview of relevant achievements published in this field from the invention of the slot waveguide to the present. The majority of transducers utilized in slot-waveguide biosensors are refractometric. Consequently, this overview has been structured according to the type of refractometric transduction configuration on which the biosensor is based, although biosensors based on other transduction methods are also considered.

A. Microring Resonators

Planar waveguide microring resonators are straightforward to design and offer high bulk and surface sensitivities while requiring a minimal footprint. They can also be integrated with other on-chip optical and fluidic components on Si chips using mass production techniques. These features make microring resonators highly suitable for use as transducers in optical biosensors, particularly for lab-on-a-chip applications [60].

The first experimental demonstration of a slot-waveguide biosensor was based on a microring resonator [61], [62]. The photonic device was fabricated in the Si_3N_4/SiO_2 material system, which, in comparison to the Si/SiO_2 system, enables the use of a wider slot region while maintaining single-mode operation. A wide slot region facilitates the filling of the slot regions with liquids for biosensing applications. The device exhibited a bulk sensitivity of 212 nm/RIU and an LoD of 16 pg/mm^2 for BSA (bovine serum albumin) detection. These values are favorably compared with those of state-of-the-art integrated photonic biosensors based on conventional waveguides, demonstrating the benefits of using slot waveguides to detect small surface modifications, such as molecular binding.

The design and fabrication of a multislot waveguide in a microring resonator are reported in [22]. The strips of the waveguide were made of SU8, an amplified electron-beam polymeric resist. By incorporating three slots in the waveguide, an increase in sensitivity of five times for homogeneous sensing and three times for surface sensing, as compared to a single slot, was demonstrated. In addition, the use of polymer materials has important advantages, such as low cost and easy fabrication. The low refractive index contrast of polymer waveguides also provides low surface scattering loss and high coupling efficiency to optical fibers.

The first experimental microring resonator slot-waveguide biosensor based on the Si/SiO_2 material system was reported in [63]. The authors used the biotin–avidin interaction as a protein detection model. The device was fabricated by using optical lithography, which represents a significant advancement toward mass-scale solutions. The slot region width was approximately 100 nm, which allowed fluid infiltration while permitting increasing sensitivity and reducing the footprint in comparison to the previously demonstrated Si_3N_4/SiO_2 counterpart.

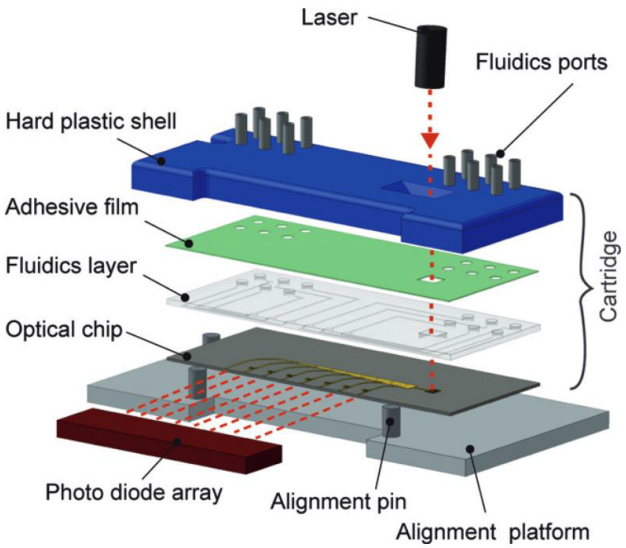

Fig. 7. Slot-waveguide biosensor array in a lab-on-a-chip system. The sensor cartridge is composed of four permanently bonded layers: the optical chip, the microfluidic layer, the adhesive film, and the hard plastic shell. Light is coupled in from the top via a surface grating coupler, and collected at the long edge of the optical chip by imaging the output facet on a 1-D InGaAs photodiode array. Reprinted with permission from [64].

The utilization of slot-waveguide biosensors in a lab-on-a-chip system was demonstrated in [64]. The authors presented the design, fabrication, and characterization of an array of optical slot-waveguide ring resonator sensors, integrated with microfluidic sample handling in a compact cartridge, for multiplexed real-time label-free biosensing (Fig. 7). The slot waveguides were fabricated in the Si_3N_4/SiO_2 material system. These devices exhibited performance improvements in terms of both bulk and surface sensing as compared to the first Si_3N_4/SiO_2 slot-waveguide ring resonator biosensor, which was attributed mainly to the reduced system noise. The achieved surface mass density detection limit is 0.9 pg/mm^2. This article demonstrates that biosensors exploiting the enhancement of light–matter interaction due to photonic slot waveguides are sufficiently mature for integration in complex platforms such as lab-on-chip microsystems and point-of-care tests.

The sensitivity of microring resonators to temperature variations may have a limiting effect on the performance of derived biosensors. In this regard, biosensors that employ silicon nitride slot-waveguide ring resonators with a temperature coefficient as low as 0.006 nm/°C were reported in [65]. The temperature coefficient is one order of magnitude smaller than that of Si counterparts. The biosensors were used to demonstrate the detection of prostate-specific antigen (PSA) with an LoD of about 50 ng/mL. Si-tagged protein G was used to anchor anti-PSA bioreceptors on the silicon nitride surfaces.

One of the principal disadvantages of slot waveguides in comparison to strip waveguides is the higher optical losses resulting from surface scattering. An innovative approach for addressing this critical aspect was demonstrated in [66]. The demonstration involved a hybrid waveguide ring resonator refractive index sensor comprising silicon slot and strip

waveguides. This configuration combines the advantages of both waveguide types, thus providing high sensitivity while maintaining low optical losses. This resulted in a high value of a figure of merit that links the optical losses with the resonator sensitivity. Using a similar approach, a double-ring resonator design with two bus waveguides that employs a hybrid strip-slot waveguide is reported in [67].

A number of additional studies have been conducted on the design and optimization of slot-waveguide ring resonators for biosensing. For instance, an accurate analysis of the optimal dimensions of a Si/SiO_2 slot-waveguide ring resonator for the detection of DNA hybridization through computer simulations can be found in [68]. Comprehensive analyses and optimizations of Si/SiO_2 refractometric sensors based on multiple-slot ring resonators are reported in [42] and [69]. The authors of these studies investigated the impact of various parameters, including waveguide dimensions and ring radius (bend effect), on the sensitivity of these multiple-slot structures.

An analysis of a Si/SiO_2 slot-waveguide microring resonator utilizing a bent asymmetric directional coupler is presented in [70]. The coupler configuration improves optical coupling between the bus (strip waveguide) and the microring (slot waveguide) and provides a more compact structure as compared to the use of a straight point-coupled directional coupler.

A novel type of waveguide comprising an SWG within a waveguide core was demonstrated in [71]. Unlike line defects in 2-D photonic crystal lattices, the light is confined within the core of the SWG, which is covered with a cladding material of a lower refractive index, as in a conventional index-guided structure. These structures permit high interaction with surrounding low-index materials, making them suitable for biosensing applications [72]. The combination of SWG and slot waveguides would therefore be expected to produce a highly sensitive biosensor, as demonstrated in [73]. The authors implemented an optical biosensor based on a multislot SWG waveguide fabricated by etching multiple trenches in a Si ring resonator in both longitudinal and transverse directions, resulting in what the authors called a multibox structure. The sensor's sensitivity was significantly increased because the optical power was largely concentrated in the gaps between the Si segments, which greatly enhances the overlap between the evanescent field and analyte. The biosensing capability of the device was demonstrated using a standard sandwich assay to investigate biomolecule interactions with both specific and nonspecific targets. The experimentally demonstrated surface sensitivity is 1900 pm/nm.

B. Interferometers

In interferometric biosensors, two nearly equivalent light paths are compared optically. One path is used to interrogate the refractive index change caused by a bioconjugate interaction, while the other serves as a reference that cancels out any nonspecific interactions. Interferometers have the capacity to detect refractive index changes of 10^{-7} RIU, which corresponds to ppb concentrations of small molecules, pg/mL concentrations of toxins and proteins, and 100–1000 s of whole cells, viruses, and spores [74]. Consequently, several optical interferometric designs based on slot waveguides have been proposed and demonstrated.

A directional coupler formed by two slot waveguides for refractive index sensing was theoretically analyzed and designed in [75]. The simulated device, assumed to be implemented in the Si/SiO_2 material system, was designed and optimized in order to achieve a favorable trade-off between the device length and sensitivity.

The first experimental demonstration of a slot-waveguide refractometric transducer for biosensing based on a Mach–Zehnder interferometer (MZI) is reported in [33]. The device, fabricated in the Si_3N_4/SiO_2 material system, consisted of a reference arm composed of a Si_3N_4 strip waveguide and a sensing arm composed of a Si_3N_4 slot waveguide. This work provides an excellent illustration of the impact of the distinct effective and modal refractive indexes of the slot and strip waveguides forming the MZI on the device performance. It also demonstrates how this asymmetry can be exploited to optimize the interferometer design for refractive index sensing and to achieve athermal performance. Although the authors did not immobilize a biological receptor on the waveguide surface to build an actual biosensor, they measured a device surface detection limit of 1.30 pg/mm^2 by depositing a polyelectrolyte multilayer film, while achieving a low temperature dependence of 5.0 pm/°C.

An actual MZI slot-waveguide biosensor manufactured by immobilizing biomolecule receptors on the sensing arm of the device, which was based on the Si_3N_4/SiO_2 material system, is documented in [76]. The authors initially investigated the biosensing capabilities of the sensor using biotin-streptavidin as a model system. Subsequently, they detected and quantified a methylated death-associated protein kinase (DAPK) gene. The limits of detection exhibited by this device for streptavidin and the methylated DNA sequence were several orders of magnitude lower than those reported for other biosensors based on integrated optics. The authors showed that methylation sequences of DAPK gene can be quantified and discriminated even at a concentration as low as 1 nM.

A novel configuration of an interferometric biosensor based on slot waveguides is demonstrated in [77]. These authors employed a double-slot hybrid plasmonic (DSHP) waveguide as a sensing arm of a MZI. The DSHP waveguide consisted of two nanoslots between a central Si strip and two lateral metal (Ag) strips on a SiO_2 layer. The authors' analysis indicated that the DSHP waveguide exhibited superior performance in terms of propagation loss and sensitivity compared to a pure plasmonic slot waveguide. The fabricated device exhibited a bulk sensitivity as high as 1061 nm/RIU for a 40-μm long DSHP waveguide.

Theoretical analyses of polymeric slot-waveguide MZIs for optimized refractive index sensing have recently been presented in [78], [79], and [80]. These studies were motivated by the known advantages of polymeric materials in integrated photonic biosensors, such as low cost, easy device fabrication, and established surface functionalization.

Together with the MZI, the Young interferometer is the most common interferometer employed for biosensing purposes. The first demonstration of a Young interferometer refractive

index sensor based on a slot waveguide was reported in [81]. The device consisted of a Y-splitter ridge waveguide in which one arm (the sensing arm) had a region with a slot waveguide. The fabrication process was conducted in a polymer material system using a simple and low-cost molding process. The sensor exhibited a bulk refractive index detection limit of 6.4×10^{-6} RIU at a visible wavelength of 633 nm and was also able to compensate for temperature variations.

C. Photonic Crystals

Photonic crystals offer remarkable advantages for photonic sensors, such as compactness and refractive index sensitivity, properties that have been successfully exploited to implement high-performance photonic biosensors [82]. Substantial work has been focused on 2-D and 1-D photonic crystal configurations because they are easier to fabricate than 3-D structures. Two-dimensional photonic crystal waveguides are most often formed by a linear defect, which is realized by removing a single row of holes from the crystal. A slotted 2-D photonic crystal can be viewed as a low-refractive-index slot defect within the guiding region of a 2-D photonic crystal waveguide (Fig. 5). The combination of the two photonic structures, the slot waveguide and the photonic crystal, enables the confinement of light to extremely small volumes of a low-refractive-index region, a property that is particularly advantageous for biosensing applications.

A refractive index sensor combining a 2-D photonic crystal and a slot waveguide in the Si/SiO_2 system was demonstrated for the first time in [83]. The authors fabricated a slotted photonic crystal cavity and measured an extremely high bulk sensitivity of 1538 nm/RIU and a quality factor (Q) of up to 50 000. An air-slot 2-D photonic crystal cavity in the Si/SiO_2 material system was reported in [84], with a bulk refractive index sensitivity of 510 nm/RIU and an extremely small active sensing volume of only 40 aL.

The first demonstration of an actual biosensor based on a slotted 2-D photonic crystal was reported in 2011 [85]. This device was fabricated in the Si/SiO_2 system and exhibited a high sensitivity over an extremely small sensing area ($2.2\ \mu m^2$) due to the strong modal overlap with the analyte. In particular, using biotin as a bioreceptor, the detected concentration of dissolved avidin was as low as 15 nM. Considering the device sensing area, this resulted in figures of 60 pg/mm^2 and 100 ag for the detectable mass density and bound mass, respectively.

Fabrication and characterization of a Si/SiO_2-based photonic integrated circuit that includes a 2-D photonic crystal slot-cavity, waveguides, and grating couplers are reported in [86]. The authors measured Q values in excess of 7500 for circuits immersed in hexane at a near 1.5 μm operation wavelength, with a refractive index detection limit of 2.3×10^{-5} RIU.

A refractive index sensor that utilized a 2-D photonic crystal in Si that incorporated a ring-slot cavity structure with a potential high Q was studied in [87].

In addition to 2-D photonic crystal geometries, 1-D photonic crystals have been employed to implement slot-waveguide-based configurations suitable for biosensor realization. In this class of biosensors, the waveguide is not fabricated by a slot defect within the guiding region of the photonic crystal, but by placing two 1-D photonic crystal nanobeams in close proximity.

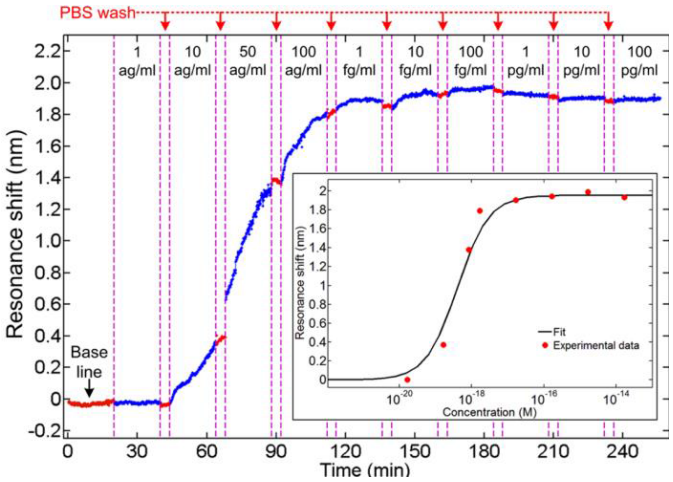

Fig. 8. Slotted 1-D PhC cavity for biosensing with LoD = 10 ag/mL. Real-time measurement of streptavidin/biotin binding shows cavity resonance wavelength shifts. Inset: Sensor calibration curve (resonance shift versus streptavidin concentration in PBS). Reprinted with permission from [90].

An InGaAsP photonic crystal slot nanobeam slow light waveguide comprising two parallel-suspended beams separated by a narrow gap, each patterned with a 1-D line of nanoholes was experimentally demonstrated in [88]. This structure, with a cavity, exhibited a bulk refractive index sensitivity as high as 900 nm/RIU.

The design, fabrication, and characterization of a high-Q slotted 1-D photonic crystal cavity on Si/SiO_2 is reported in [89]. The configuration employed a parabolic modulated width stack without reflection mirrors, exhibiting a Q-factor on the order of 10^4 and a bulk sensitivity of 410 nm/RIU. A label-free biosensor using a nanoslotted parallel multibeam photonic crystal cavity, implemented in the Si/SiO_2 system, capable of detecting 10 ag/mL of streptavidin solution was demonstrated in [90]. Fig. 8 shows the experimental results used to determine this remarkably low LoD value.

Three-dimensional computer simulations on parallel tapered nanoslotted photonic crystal nanobeam cavities were described in [91]. The results showed a bulk sensitivity of over 600 nm/RIU and an optimal Q-factor of 11 770. In addition, theoretical studies on various geometries of 1-D slotted photonic crystal nanobeams as refractometric transducers can be found in [92] and [93]. The simulations indicated that these devices are able to exhibit high bulk sensitivity, high Q, and small effective mode volume.

The fabrication and characterization of a nonsuspended multislot photonic crystal cavity sensor in the Si/SiO_2 material system were shown in [94]. The nonsuspended feature allows for the fabrication of structures with enhanced structural integrity compared to suspending configurations. The device was optimized to distribute most of the light in the multiple low index regions of the structure, achieving a high bulk sensitivity of 586 nm/RIU.

D. Bragg Gratings

The spectral response of Bragg gratings, both uniform and phase-shifted gratings, is highly sensitive to changes in the surrounding refractive index. This makes them an excellent choice for implementing refractometric biosensors. Phase-shifted gratings [95] are particularly well-suited for high-sensitivity biosensing applications due to their ability to exhibit a refractive-index-sensitive resonance peak with a high Q-value, which is advantageous for achieving low limits of detection values. The influence of grating design parameters, including grating period, fill factor, and etch depth, on the reflection bandwidth and Q-factor of these devices has been investigated by several authors, see, for example, [96], [97], [98].

Bragg gratings based on slot waveguides provide improved sensitivity due to the enhancement of the optical confinement in the low-refractive-index slot. Consequently, the investigation of these devices for biosensing has constituted a significant area of research in the field.

The design and fabrication a Bragg-grating air-slot optical waveguide on Si/SiO_2 for the purpose of label-free biosensing are presented in [99]. The Bragg grating, which was defined in the inner walls of a slot waveguide, generated a bandgap. The spectral shift of the upper band edge was employed as the sensing mechanism for fluids or biomolecules present within the slot. Although the sensitivity of this device could not be determined experimentally due to the insufficient wavelength span of the broadband source employed, the authors claimed that this device could potentially offer a sensitivity of 500 nm/RIU or higher.

An experimental demonstration of an actual biosensor based on a Si/SiO_2 phase-shifted Bragg grating in a slot waveguide can be found in [100]. In this device, the Bragg gratings were formed by corrugating the outer sidewalls of the slot waveguide, where the weak evanescent field decays. The phase shift, introduced into the middle of the gratings, leads to a sharp resonance peak (Fabry-Perot cavity with mirrors formed by two Bragg reflectors) in the transmission spectrum, which is sensitive to refractive index changes in the slot region (340 nm/RIU). The biosensing capability of the device was demonstrated by conducting a series of sandwich assays involving high-affinity biomolecules, which indicated its potential for use in clinically relevant diagnostic settings. The device was manufactured using a CMOS-compatible process, which enables mass production at a low-cost.

A phase-shifted Bragg grating based on a multibox (multislot SWG waveguide) structure was demonstrated in [101]. The device was fabricated in the Si/SiO_2 system and exhibited a Q-factor that was three times higher than that of its multibox-based microring counterpart [73], resulting in an improved detection limit. Through a biotin-streptavidin affinity assay, these authors were able to monitor a minimum detectable concentration of biotin down to 23 nM.

In a more recent study, a multislot subwavelength Bragg grating refractive index sensor in the Si/SiO_2 material system was demonstrated in [102]. The photonic structure was optimized through 3-D computer simulations. The authors fabricated a sensor of only 9.5 μm in length having a record-high bulk sensitivity of 730 nm/RIU.

Theoretical studies on refractive index Bragg grating sensors based on slot waveguides were also conducted in [103] and [104]. Wang and Madsen [103] designed and modeled a refractive index sensor based on a phase-shifted sidewall Bragg grating in a silicon slot waveguide. The Bragg gratings were defined at the inner sidewalls of the slot waveguide. The simulated device exhibited a resonance wavelength that varied linearly with the refractive index of the slot region, with a slope of 291.93 nm/RIU. The work of [104] presents a simulation of a structure that consisted of a sidewall grating in a dual slot waveguide in the Si/SiO_2 material system. By optimizing the geometric parameters of the device, it was possible to achieve high Q and high transmittivity, as well as high bulk sensitivity, which reduces the limit of detection.

E. Other Refractometric Configurations

The previously mentioned transducer configurations represent the most prevalent approach utilized in the development of waveguide-based refractometric biosensors. Nevertheless, they are not the sole option. Alternative and/or combined refractometric designs have also benefited from the integration of slot waveguides, offering both compactness and high sensitivity.

A refractive index sensor based on grating-assisted coupling between a strip waveguide and a slot waveguide in Si_3N_4/SiO_2 material system was studied at design level in [105]. The slot waveguide functioned as the sensing waveguide, whereas the strip waveguide was employed for injecting and detecting the light probe. The introduction of a grating within the strip waveguide enabled co-directional coupling between this waveguide and the slot waveguide, thus facilitating the transfer of light. For a grating period selected according to an optimal criterion, a maximum coupling is attained at a particular wavelength, which is dependent on the effective refractive index of the slot waveguide. An optimized device was predicted to exhibit a high sensitivity of approximately 1460 nm/RIU. It was also found that an isolation layer on the strip waveguide could enhance the sensitivity and mitigate the effects of temperature.

A Si/SiO_2 nanophotonic biosensor based on Fano resonance using a slot-waveguide configuration resulting from the combination of nanodisks and an SWG was reported in [106]. In this structure, the coupling of nanodisk and grating modes creates a Fano resonance profile (dip and peak) in the transmission spectrum, which is highly sensitive to bulk refractive index changes (1463 nm/RIU). Furthermore, the asymmetric line shape and narrow linewidth of the Fano resonance provides a high quality factor.

Theoretical investigation of a refractive photonic sensor that integrates a slot microring resonator and a slot phase-shifted sidewall Bragg grating within the Si/SiO_2 material system can be found in [107]. The Bragg grating was employed as a bus to convey light to/from the ring resonator, while the sensing area included the slot regions of both the grating and the ring. The simulated device exhibited a high quality factor and a wide operating bandwidth.

A Si/SiO_2 slot-waveguide microring resonator containing four evenly distributed holes perforated in the outer Si rail of the ring slot waveguide is presented in [108]. In this structure, each pair of holes can be regarded as a Fabry-Perot resonator, which exhibits optical modes that interact and interfere with the ring resonator modes. This results in a phenomenon of resonance splitting, which enhances the overall quality factor and therefore the resolution of the sensor.

A Si/SiO_2 slot-waveguide microring resonator with a grating defined in the inner sidewall of the inner rail of the ring slot waveguide was proposed and studied in [109]. The combination of the microring resonator and the diffraction grating results in a transmission spectrum that can be regarded as the result of two filtering processes, which allows for enlarging the operating range of the sensor due to good suppression of side modes.

F. Slot-Waveguide Refractive Index Sensitivity Studies

In addition to the reports on specific transducer configurations that have been presented thus far, a number of studies have been conducted on the sensing performance of generic slot waveguides, which could be employed to implement one or more of the refractometric architectures that have been discussed. These investigations are typically focused on identifying the optimal geometrical and dimensional parameters of slot waveguides to achieve the highest bulk and surface waveguide sensitivities in a particular material system.

In this regard, the initial study was reported in [110]. The authors conducted theoretical investigations of Si/SiO_2 slot waveguides for chemical and biochemical sensing. The modal and confinement properties of slot waveguides were studied, considering geometrical factors and fabrication tolerances, and compared to those of conventional strip and rib waveguides. Their findings demonstrated that the homogeneous sensitivity value exhibited by slot waveguides is larger than those obtained by other nanometer guiding structures. In particular, this article defines the waveguide sensitivity in the case of homogeneous sensing S_h as the derivative of the effective index of the propagating mode with respect to the cover medium refractive index. This article proved, for the first time, that, in slot waveguides, S_h can also exceed 1 for the quasi-TE modes supported by silicon slot waveguides with optimized geometric sizes. For silicon strip and rib waveguides, the maximum value of S_h that is realistically achievable for both the quasi-TE and the quasi-TM modes does not exceed 0.7.

An analysis of mode confinement properties in slot waveguides realized in low-refractive-index materials is reported in [111]. The authors found that a slot volume, even when filled with a liquid with a refractive index higher than that of the waveguide strips, always enables an optimum overlap between the analyte (contained in the liquid) and the guided mode. They concluded that a careful design of a multiple-slot waveguide made of low-refractive-index materials, such as polymers, allows for homogeneous sensitivities comparable to those achievable in high refractive index semiconductor material systems.

The refractive index sensitivity of a polymer slot waveguide coated with a bilayer of Al_2O_3/TiO_2 was investigated theoretically in [112]. The high refractive index Al_2O_3 and TiO_2 layers had thicknesses of the order of several tens of nanometers and were assumed to be formed on the sidewalls of the polymer rails by atomic layer deposition. The simulations indicated that the incorporation of these thin layers offered a significant improvement in the confinement factor and sensitivity at visible wavelengths as compared to those of an uncoated polymer slot waveguide.

A horizontal slot waveguide for refractometric detection of DNA hybridization was studied in [113]. The high index regions of the slot waveguide were assumed to be made of polysilicon layers. The simulations considered single-stranded DNA (ssDNA) molecules as bioreceptors and complementary DNA (c-DNA) molecules by introducing homogeneous refractive index nanometric layers in the sensitive region of the modeled structure. The waveguide dimensions were optimized in order to achieve the maximum sensitivity for ssDNA-cDNA binding. The optimized horizontal slot waveguide was studied as a part of both, an MZI and a ring resonator for high-performance refractometric DNA sensing.

A Si/SiO_2 cross-slot waveguide configuration that includes both vertical and horizontal slots was proposed and simulated in [114]. This waveguide architecture allows power enhancement in the slot region for both quasi-TE and quasi-TM polarizations. The authors' simulations indicate that the bulk sensitivity of this waveguide can be almost twice that of vertical and horizontal slot waveguides with similar dimensions. Additionally, a nearly polarization-independent cross-slot waveguide can be obtained by proper design of the Si strips.

Simulation studies on a Si/SiO_2 SWG double-slot waveguide refractometric transducer were reported in [115]. The authors studied and compared the modal characteristics of SWG ridge, single-slot, and double-slot SWGs and modeled the spectral characteristics of a ring resonator based on the aforementioned waveguides. The authors concluded that the SWG double-slot ring resonator exhibited superior performance compared to those based on the other waveguiding structures.

G. Nonrefractometric Configurations

Although the majority of reported optical transducers based on slot waveguides for biosensing have been of the refractometric type, a few works on other transducer schemes, such as absorption/fluorescence and opto-mechanical transducing methods, and spectrometric techniques such as surface-enhanced Raman spectroscopy (SERS) based on slot waveguides have also been reported.

A theoretical investigation on the light excitation and light collection efficiencies of 2-D slot waveguides can be found in [116]. The authors considered excitation and collection wavelengths of 633 and 690 nm, respectively, and refractive indexes of 2 and 1.33 for the high-index rails and low-index slot region, respectively. A slot waveguide could improve both the excitation and collection efficiencies with respect to a single slab waveguide due to the enhanced **E**-field intensity at the rail/slot interfaces. In a related vein, the aforementioned work reported in [111] on low-index slot waveguides also

considered relevant issues pertaining to the integration of slot waveguides for evanescent absorption and fluorescence analysis.

The optical performance of a slot waveguide is highly sensitive to both variations in the refractive index of the slot region and to small changes in the distance between the slots. This property was utilized to propose and analyze a nanomechanical optical deflection sensor consisting of a disk resonator formed by a $Si_3N_4/SiO_2/Si$ horizontal slot waveguide [117]. The Si_3N_4 layer served as a circular cantilever supported by a smaller-radius SiO_2 disk. Differential surface stress in the Si_3N_4 cantilever due to molecular recognition on one of its surfaces produces the bending (deflection) of the cantilever, which in turn alters the slot distance and consequently the optical response of the disk resonator. A deflection sensitivity of 33 nm^{-1} was calculated, which is approximately four orders of magnitude greater than those of state-of-the-art microcantilever sensors.

Raman spectroscopy permits the direct identification and quantification of molecules based on their vibrational characteristics, which are uniquely determined by their molecular structure. This approach has proven to be a highly successful methodology in biosensing applications [118]. Waveguide-enhanced Raman spectroscopy (WERS), a novel approach to enhancing the sensitivity of Raman scattering, exploits the interaction between analytes and the evanescent field of a waveguide on a photonic chip, with the aim of addressing challenges associated with SERS [119]. This includes reproducibility and robustness, two key limitations of SERS. The demonstration that the quasi-TE mode of a slot waveguide can provide greater WERS efficiency than both the TE and TM modes for a rectangular waveguide can be found in [120]. A Si_3N_4 slot-waveguide WERS sensor for the detection of organic pollutants in water was reported in [121]. Mesoporous silica modified by hexamethyldisilazane (HMDS) was utilized as the top cladding to absorb and enrich pollutants in the aqueous sample by a factor of 600, which further enhanced the sensitivity of the device. A study on the use of a nanoplasmonic slot waveguide as a waveguide SERS substrate is reported in [122]. The SERS substrate was able to detect trypsin using a reproducible and reliable platform suitable for lab-on-a-chip applications.

IV. Gas Sensing

On-chip gas sensing based on integrated microphotonics is currently generating considerable attention due to their potential for high sensitivity, compactness, and seamless integration with other electronic and photonic systems. The sensors operate based on several principles, including refractive index change, Raman spectroscopy, infrared absorption, cavity ring-down spectroscopy, and photothermal spectroscopy. Each method offers distinct advantages depending on the application and the specific gas to be detected [123]. Slot waveguide-based gas sensors represent a very promising class of on-chip optical gas sensors that exploit the above-discussed unique properties of slot waveguides to enhance light–matter interactions. The design of slot waveguides allows a significant portion of the optical mode to be concentrated in a low-index region, where the target gas is present. This enhances the interaction between light and gas molecules, leading to increased sensitivity. The heightened sensitivity of slot waveguide-based sensors is particularly valuable for applications requiring the detection of low gas concentrations.

The concept of using slot waveguides for gas sensing was first demonstrated through the use of a ring resonator structure incorporating Si/SiO_2 slot waveguides [124]. The use of a resonating structure is especially beneficial in this context as it permits the accumulation of optical power within the resonator, thereby further amplifying the sensor's sensitivity. The slot width was as small as 40 nm, leading to very high E-field enhancement in the slot region. The bulk sensitivity of this device was measured to be as high as 490 nm/RIU, evidencing larger light–fluid interaction than that obtained with Si_3N_4/SiO_2 slot waveguides. As a proof-of-concept, the sensor was utilized to detect small changes in the refractive index of acetylene gas due to composition and pressure. A minimum detectable change in the refractive index of 10^{-4} RIU was experimentally proved. An on-chip gas sensor exploiting the same operating principle and capable of detecting ethanol vapor with LoD = 25 ppm was experimentally demonstrated in [125]. The ring resonator has a racetrack shape with a radius of 5 μm and a straight waveguide length of 3 μm. The ring was coated with a ZnO nanoparticle film and the resonance wavelength shift, which allows for the gas concentration estimation, is due to the adsorption of ethanol by the ZnO nanocrystals. The relationship between the measured shift in the resonance wavelength and the ethanol concentration is nonlinear, being well fit by a Langmuir isotherm. The relationship is approximately linear up to the ethanol concentration of 100 ppm. A saturation effect is observed for larger values of the concertation.

The use of an air-slot PhC resonant cavity in the context of gas sensing was experimentally explored in [84]. The achieved bulk sensitivity of the cavity, with a Q-factor of 26 000, was 510 nm/RIU, which is similar to that attainable with ring resonators, and the minimum detectable change in the refractive index is of the order of 10^{-5} RIU.

The efficacy of photonic crystal slot waveguides in enhancing gas sensing capabilities through increased interaction lengths and light–gas interaction was proved by two noteworthy studies based on near-IR absorption spectroscopy and achieving LoD values down to 100 ppb [126], [127]. The integration of these on-chip technologies offers a promising route for developing compact, efficient, and sensitive sensors for gas detection in various environmental and industrial contexts.

The sensor reported in [126], which is 300 μm in length, was intended for measuring methane gas. The device design combines slow light propagation and high electric field intensity within a narrow 90 nm low-index slot, significantly extending the effective optical path length for enhanced sensitivity. Methane concentrations as low as 100 ppm were successfully detected. The high sensitivity can be attributed to the use of the SOI platform, which enabled the manufacturing of a line defect waveguide that operates under slow light conditions with a group index of about 30 near the methane

absorption peak at 1665.5 nm. The device exhibited a group velocity slowdown factor of approximately 100, significantly enhancing the electric field overlap with the analyte.

The device reported in [127] was intended for detecting organic contaminants in water. This device, also based on a silicon photonic crystal slot waveguide, is 300 μm long and uses a 75-nm wide slot for high electric field intensity, thus extending the effective absorption path length for improved sensitivity. The system is optimized for xylene detection in water, utilizing a polydimethylsiloxane (PDMS) cladding that enhances the sensitivity to xylene by providing a hydrophobic environment, thereby preventing interference from water absorption. The slot-waveguide structure, with a group index of approximately 40 at specific xylene absorption peaks, allows for effective slow light propagation, optimizing light–analyte interaction. The detection limit achieved was 100 ppb for xylene, corresponding to 86 μg/L.

A low value of LoD has been achieved using diamond PhC cavities in gas sensing, demonstrating their high sensitivity and selectivity [128]. The fabricated diamond resonators utilize a slotted design in a width-modulated waveguide, which enhances light–matter interaction by confining optical modes tightly within the low-refractive-index regions. The devices are responsive to changes in the refractive index of the surrounding gaseous environment, achieving a wavelength sensitivity of up to 350 nm/RIU. This specificity/selectivity of the sensor was achieved through surface functionalization of the diamond, specifically using oxidized surface terminations, which significantly enhances affinity for polar molecules such as hexanol. In the experiments, the PhC cavities were exposed to hexanol vapor in a controlled environment, with the diamond surface demonstrating a resonance wavelength shift of 7.5 pm per ppm of hexanol. The detection limit was found to be as low as 1.3 ppm, indicating the capability of detecting trace amounts of gas. For nonpolar molecules like pentane, the sensitivity was markedly lower, with a shift of 0.04 pm/ppm, demonstrating the specificity of the oxidized diamond surface to polar molecules. The diamond PhC devices showed a Q-factor of 5400, limited primarily by the scattering losses at grain boundaries in the polycrystalline diamond.

To date, one of the most promising achievements in the field of slot-based on-chip gas sensing was reported in [129]. The experimental study is focused on an advanced approach to methane sensing using mid-IR slot waveguides, achieving a detection limit of 0.3 ppm (Fig. 9). This represented a significant improvement over the state-of-the-art in on-chip spectroscopy, with an LoD that is two orders of magnitude lower than previous reports. The slot-waveguide design utilized an SOI platform with a 500-nm thick silicon layer atop a 3-μm thick buried oxide layer. The waveguide geometry is characterized by a narrow air slot, 150 nm wide. This configuration maximizes the optical confinement factor in air—the fraction of optical mode power confined in the low-index air region—while minimizing losses. A confinement factor in air of 79% was achieved, which is crucial for enhancing the light–matter interaction within the air slot, thereby improving methane detection sensitivity.

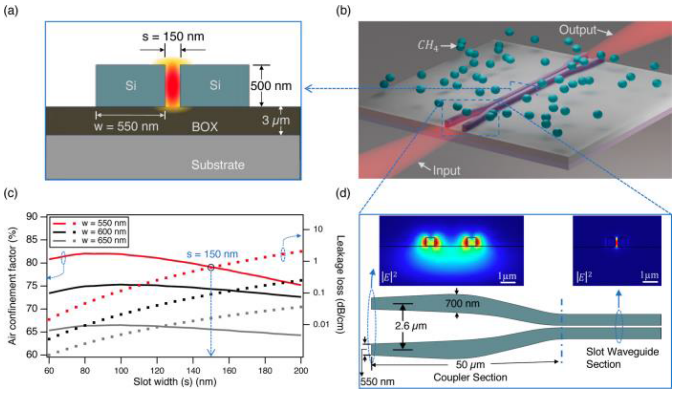

Fig. 9. Overview of the components and characteristics of the slot-waveguide gas sensor chip with LoD = 0.3 ppm. (a) Cross section of the slot waveguide. (b) Layout of the sensor chip. The chip is 1 cm^2 in size with straight waveguides measuring 1.15 cm in length. (c) Simulated air confinement factor (solid lines) and the leakage loss into the substrate (dotted lines) as a function of slot width (s) for different strip widths (w). (d) Design of the double-tip coupler, with simulated mode profiles at the coupler facet and across the slot waveguide. Reprinted with permission from [129].

The experimental setup involved the integration of the slot waveguide within a laser absorption spectroscopy system operating at a wavelength of 3270.4 nm, targeting a specific methane absorption line. The use of double-tip couplers at the waveguide facets effectively suppressed etalon fringes, reducing unwanted reflections to approximately 0.006% per interface, thus minimizing noise and enhancing the stability of the measurement. The waveguide length was optimized at 1.15 cm to balance the trade-off between interaction length and propagation loss. The propagation loss was measured to be 8.3 $\pm$ 0.3 dB/cm, which is attributed primarily to absorption by water adsorbed on the waveguide surface. The study highlighted that water adsorption significantly impacts performance, especially given the overlap between methane and water absorption bands in the MIR region. By heating the waveguide to 115 °C and flushing it with nitrogen, the researchers were able to reduce these losses, demonstrating the importance of surface treatment in improving sensor performance. Methane detection was conducted under controlled conditions, with methane concentrations varying between 0 and 1000 ppm. In this wide dynamic range, the sensor response has been very linear.

In addition to the above-mentioned experimental results in the last decade, several theoretical papers have studied the potential of photonic slot waveguides in the context of on-chip gas sensing in both the near-IR and the mid-IR [130], [131], [132], [133], [134], [135], [136]. Collectively, these studies investigate the diverse applications and configurations of photonic slot waveguides for gas sensing. The simulations and the reported designs further confirm that tailoring the waveguide properties, such as slot width, waveguide material, and structural design, allows for the optimization of sensitivity, selectivity, and detection limits for specific gases.

A sealed slot-waveguide gas sensor with a design optimized for minimal sample volume was developed in [135]. This

sensor was intended to operate at a wavelength of 1550 nm with a high sensitivity of 1000 nm/RIU. Based on simulations, the sensor would detect ammonia gas at concentrations as low as 2 ppm. The sealed design effectively isolates the sensing region from external environmental influences, ensuring high precision in confined spaces, which is critical for applications requiring minimal sample volumes.

Slow-light Bloch slot waveguides (BSWs) were investigated theoretically to improve gas sensing performance by increasing the group index through SWG engineering [136]. The simulations predicted an LoD of 0.034 ppm for methane detection in the near-infrared and 0.29 ppm in the mid-infrared at an optimal propagation length of 1.45 cm. These results show the capability of BSWs to enhance light–gas interactions and achieve ultralow detection limits by maximizing both spatial and temporal interactions between light and the gas molecules.

V. Conclusion

This article highlights the significant advancements in photonic slot waveguides for both biosensing and gas sensing applications, emphasizing their potential for on-chip integration and high sensitivity. Photonic slot waveguides, with their ability to enhance light–matter interactions by confining the optical field within low-refractive-index regions, have facilitated the design and experimental demonstration of high-performance sensors. Recent experimental results comparing four different ring configurations in terms of figure-of-merit and showing that the slotted ring performs better than competitive approaches further confirm this well-established achievement [137].

In biosensing, the lowest LoD achieved using slot waveguide-based devices is currently 10 ag/mL, as demonstrated experimentally for streptavidin detection in phosphate-buffered saline solutions. This level of sensitivity significantly surpasses traditional methods, underscoring the capability of slot waveguides to detect extremely low concentrations of biomolecules. Such sensitivity is crucial in medical diagnostics, where early detection of disease markers can lead to more effective treatment. Photonic slot waveguides are particularly suited for integration into lab-on-a-chip devices for applications such as liquid biopsy, enabling minimally invasive cancer diagnostics by detecting tumor-derived biomarkers in body fluids.

For gas sensing, photonic slot waveguides have demonstrated exceptional performance, especially in detecting gases at near-IR and mid-IR wavelengths. LoD values of the order of 100 ppb have been achieved for xylene and methane detection, showing the high sensitivity and specificity of these waveguides. This capability is pivotal for environmental monitoring and industrial safety, where detecting trace amounts of hazardous gases can prevent accidents and mitigate environmental impact. Furthermore, slot waveguides show great promise in breath analysis and breath biopsy applications, which are emerging as powerful noninvasive diagnostic tools.

Overall, the integration of photonic slot waveguides into chip-scale sensors has been demonstrated as a versatile platform for both biosensing and gas sensing applications, enabling the development of compact, low-cost, and highly sensitive devices. The capacity to tailor the waveguide design for specific applications further enhances their utility, positioning them as a promising technology for future on-chip sensing solutions. Beyond medical diagnostics and environmental monitoring, these sensors hold potential for use in food safety, homeland security, and other fields requiring sensitive, real-time detection capabilities.

Future developments in photonic slot waveguide-based sensing should consider the influence of the analyte matrix (e.g., gaseous, liquid, aqueous, plasma, humidity) on various sensing mechanisms, such as resonators, interferometers, and photonic crystals, to optimize sensor performance across different application scenarios.

References

[1] Q. Liu, *Portable and Wearable Sensing Systems: Techniques, Fabrication, and Biochemical Detection*. Weinheim, Germany: Wiley-VCH, 2024.

[2] R. Bawa, G. F. Audette, S. R. Bawa, B. Patel, B. D. Johnson, and R. Khanna, Eds., *Advances in Medical Imaging, Detection, and Diagnosis*. Singapore: Jenny Stanford Publishing, 2023.

[3] C. Alix-Panabières and K. Pantel, "Circulating tumor cells: Liquid biopsy of cancer," *Clin. Chem.*, vol. 59, no. 1, pp. 110–118, Jan. 2013, doi: 10.1373/clinchem.2012.194258.

[4] C. Alix-Panabières and K. Pantel, "Clinical applications of circulating tumor cells and circulating tumor DNA as liquid biopsy," *Cancer Discovery*, vol. 6, no. 5, pp. 479–491, May 2016, doi: 10.1158/2159-8290.CD-15-1483.

[5] F. Dell'Olio, J. Su, T. Huser, V. Sottile, L. E. Cortés-Hernández, and C. Alix-Panabières, "Photonic technologies for liquid biopsies: Recent advances and open research challenges," *Laser Photon. Rev.*, vol. 15, no. 1, Jan. 2021, Art. no. 2000255, doi: 10.1002/lpor.202000255.

[6] G. Ferrandino et al., "Breath biopsy assessment of liver disease using an exogenous volatile organic compound—Toward improved detection of liver impairment," *Clin. Transl. Gastroenterol.*, vol. 11, no. 9, Sep. 2020, Art. no. e00239, doi: 10.14309/ctg.0000000000000239.

[7] B. Abderrahman, "Exhaled breath biopsy: A new cancer detection paradigm," *Future Oncol.*, vol. 15, no. 15, pp. 1679–1682, May 2019, doi: 10.2217/fon-2019-0091.

[8] E. Petryayeva and W. R. Algar, "Toward point-of-care diagnostics with consumer electronic devices: The expanding role of nanoparticles," *RSC Adv.*, vol. 5, no. 28, pp. 22256–22282, 2015, doi: 10.1039/c4ra15036h.

[9] P. B. Luppa, C. Müller, A. Schlichtiger, and H. Schlebusch, "Point-of-care testing (POCT): Current techniques and future perspectives," *TrAC Trends Anal. Chem.*, vol. 30, no. 6, pp. 887–898, Jun. 2011, doi: 10.1016/j.trac.2011.01.019.

[10] W. Jung, J. Han, J.-W. Choi, and C. H. Ahn, "Point-of-care testing (POCT) diagnostic systems using microfluidic lab-on-a-chip technologies," *Microelectron. Eng.*, vol. 132, pp. 46–57, Jan. 2015, doi: 10.1016/j.mee.2014.09.024.

[11] N. R. Abdulhalim, Ed., "Optical Guided-wave Chemical and Biosensors. 1/with contrib," in *Springer Series on Chemical Sensors and Biosensors*, N. R. Abdulhalim, 1st ed., Dordrecht, The Netherlands: Springer, 2009.

[12] M. Zourob and A. Lakhtakia, Eds., "Optical guided-wave chemical and biosensors II," in *Springer Series on Chemical Sensors and Biosensors*. Berlin, Germany: Springer, 2010.

[13] M. C. Estevez, M. Alvarez, and L. M. Lechuga, "Integrated optical devices for lab-on-a-chip biosensing applications," *Laser Photon. Rev.*, vol. 6, no. 4, pp. 463–487, Jul. 2012, doi: 10.1002/lpor.201100025.

[14] A. L. Washburn and R. C. Bailey, "Photonics-on-a-chip: Recent advances in integrated waveguides as enabling detection elements for real-world, lab-on-a-chip biosensing applications," *Analyst*, vol. 136, no. 2, pp. 227–236, 2011, doi: 10.1039/C0AN00449A.

[15] C. Dhote, A. Singh, and S. Kumar, "Silicon photonics sensors for biophotonic applications—A review," *IEEE Sensors J.*, vol. 22, no. 19, pp. 18228–18239, Oct. 2022, doi: 10.1109/JSEN.2022.3199663.

[16] J. Wang, M. M. Sanchez, Y. Yin, R. Herzer, L. Ma, and O. G. Schmidt, "Silicon-based integrated label-free optofluidic biosensors: Latest advances and roadmap," *Adv. Mater. Technol.*, vol. 5, no. 6, Jun. 2020, Art. no. 1901138, doi: 10.1002/admt.201901138.

[17] V. J. Cadarso, C. Fernández-Sánchez, A. Llobera, M. Darder, and C. Domínguez, "Optical biosensor based on hollow integrated waveguides," *Anal. Chem.*, vol. 80, no. 9, pp. 3498–3501, May 2008, doi: 10.1021/ac702293r.

[18] R. Bernini, E. De Nuccio, A. Minardo, L. Zeni, and P. M. Sarro, "Integrated silicon optical sensors based on hollow core waveguide," *Proc. SPIE*, vol. 6477, Feb. 2007, Art. no. 647714, doi: 10.1117/12.700410.

[19] V. R. Almeida, Q. Xu, C. A. Barrios, and M. Lipson, "Guiding and confining light in void nanostructure," *Opt. Lett.*, vol. 29, no. 11, p. 1209, Jun. 2004, doi: 10.1364/ol.29.001209.

[20] Q. Xu, V. R. Almeida, R. R. Panepucci, and M. Lipson, "Experimental demonstration of guiding and confining light in nanometer-size low-refractive-index material," *Opt. Lett.*, vol. 29, no. 14, p. 1626, Jul. 2004, doi: 10.1364/ol.29.001626.

[21] C. A. Barrios et al., "Demonstration of slot-waveguide structures on silicon nitride/silicon oxide platform," *Opt. Exp.*, vol. 15, no. 11, p. 6846, 2007, doi: 10.1364/oe.15.006846.

[22] H. Sun, A. Chen, and L. R. Dalton, "Enhanced evanescent confinement in multiple-slot waveguides and its application in biochemical sensing," *IEEE Photon. J.*, vol. 1, no. 1, pp. 48–57, Jun. 2009, doi: 10.1109/JPHOT.2009.2025602.

[23] Y. Enami, B. Yuan, M. Tanaka, J. Luo, and A. K.-Y. Jen, "Electro-optic polymer/TiO_2 multilayer slot waveguide modulators," *Appl. Phys. Lett.*, vol. 101, no. 12, Sep. 2012, Art. no. 123509, doi: 10.1063/1.4754597.

[24] F. Qiu et al., "A hybrid electro-optic polymer and TiO_2 double-slot waveguide modulator," *Sci. Rep.*, vol. 5, no. 1, p. 8561, Feb. 2015, doi: 10.1038/srep08561.

[25] A. Di Falco, C. Conti, and G. Assanto, "Quadratic phase matching in slot waveguides," *Opt. Lett.*, vol. 31, no. 21, p. 3146, Nov. 2006, doi: 10.1364/ol.31.003146.

[26] G. Veronis and S. Fan, "Modes of subwavelength plasmonic slot waveguides," *J. Lightw. Technol.*, vol. 25, no. 9, pp. 2511–2521, Sep. 2007, doi: 10.1109/jlt.2007.903544.

[27] S. Zhu, G. Q. Lo, and D. L. Kwong, "Theoretical investigation of silicon MOS-type plasmonic slot waveguide based MZI modulators," *Opt. Exp.*, vol. 18, no. 26, p. 27802, Dec. 2010, doi: 10.1364/oe.18.027802.

[28] S. Zhu, G. Q. Lo, and D. L. Kwong, "Experimental demonstration of horizontal nanoplasmonic slot waveguide-ring resonators with submicrometer radius," *IEEE Photon. Technol. Lett.*, vol. 23, no. 24, pp. 1896–1898, Dec. 15, 2011, doi: 10.1109/LPT.2011.2171934.

[29] H. Kogelnik, "Theory of optical waveguides," in *Guided-Wave Optoelectronics* (Springer Series in Electronics and Photonics), vol. 26, T. Tamir, Ed., Berlin, Germany: Springer, 1988, pp. 7–88, doi: 10.1007/978-3-642-97074-0_2.

[30] L. Zhang, Y. Yue, R. G. Beausoleil, and A. E. Willner, "Flattened dispersion in silicon slot waveguides," *Opt. Exp.*, vol. 18, no. 19, p. 20529, Sep. 2010, doi: 10.1364/oe.18.020529.

[31] H. Ryu, J. Kim, Y. M. Jhon, S. Lee, and N. Park, "Effect of index contrasts in the wide spectral-range control of slot waveguide dispersion," *Opt. Exp.*, vol. 20, no. 12, p. 13189, Jun. 2012, doi: 10.1364/oe.20.013189.

[32] R. Ding et al., "Low-loss strip-loaded slot waveguides in silicon-on-insulator," *Opt. Exp.*, vol. 18, no. 24, p. 25061, Nov. 2010, doi: 10.1364/oe.18.025061.

[33] X. Tu et al., "Thermal independent silicon-nitride slot waveguide biosensor with high sensitivity," *Opt. Exp.*, vol. 20, no. 3, p. 2640, Jan. 2012, doi: 10.1364/oe.20.002640.

[34] M. Hiltunen et al., "Polymeric slot waveguide at visible wavelength," *Opt. Lett.*, vol. 37, no. 21, p. 4449, Nov. 2012, doi: 10.1364/ol.37.004449.

[35] P. A. Anderson, B. S. Schmidt, and M. Lipson, "High confinement in silicon slot waveguides with sharp bends," *Opt. Exp.*, vol. 14, no. 20, p. 9197, 2006, doi: 10.1364/oe.14.009197.

[36] S. Mas, J. Caraquitena, J. V. Galán, P. Sanchis, and J. Martí, "Tailoring the dispersion behavior of silicon nanophotonic slot waveguides," *Opt. Exp.*, vol. 18, no. 20, p. 20839, Sep. 2010, doi: 10.1364/oe.18.020839.

[37] R. Sun et al., "Horizontal single and multiple slot waveguides: Optical transmission at λ = 1550 nm," *Opt. Exp.*, vol. 15, no. 26, p. 17967, 2007, doi: 10.1364/oe.15.017967.

[38] K. Preston and M. Lipson, "Slot waveguides with polycrystalline silicon for electrical injection," *Opt. Exp.*, vol. 17, no. 3, p. 1527, Feb. 2009, doi: 10.1364/oe.17.001527.

[39] R. M. Pafchek, J. Li, R. S. Tummidi, and T. L. Koch, "Low loss Si-SiO_2-Si 8nm slot waveguides," in *Proc. Conf. Lasers Electro-Opt.*, San Jose, CA, USA, May 2008, pp. 1–2, doi: 10.1109/CLEO.2008.4551525.

[40] R. Guider, N. Daldosso, A. Pitanti, E. Jordana, J.-M. Fedeli, and L. Pavesi, "NanoSi low loss horizontal slot waveguides coupled to high Q ring resonators," *Opt. Exp.*, vol. 17, no. 23, p. 20762, Nov. 2009, doi: 10.1364/oe.17.020762.

[41] N.-N. Feng, J. Michel, and L. C. Kimerling, "Optical field concentration in low-index waveguides," *IEEE J. Quantum Electron.*, vol. 42, no. 9, pp. 883–888, Sep. 2006, doi: 10.1109/JQE.2006.880061.

[42] I. Khodadad, N. Clarke, M. Khorasaninejad, D. Henneke, and S. S. Saini, "Optimization of multiple-slot waveguides for biochemical sensing," *Appl. Opt.*, vol. 53, no. 23, p. 5169, Aug. 2014, doi: 10.1364/ao.53.005169.

[43] A. Di Falco, L. O'Faolain, and T. F. Krauss, "Photonic crystal slotted slab waveguides," *Photon. Nanostruct. Fundam. Appl.*, vol. 6, no. 1, pp. 38–41, Apr. 2008, doi: 10.1016/j.photonics.2007.08.001.

[44] A. Di Falco, L. O'Faolain, and T. F. Krauss, "Dispersion control and slow light in slotted photonic crystal waveguides," *Appl. Phys. Lett.*, vol. 92, no. 8, Feb. 2008, Art. no. 083501, doi: 10.1063/1.2885072.

[45] A. Di Falco, M. Massari, M. G. Scullion, S. A. Schulz, F. Romanato, and T. F. Krauss, "Propagation losses of slotted photonic crystal waveguides," *IEEE Photon. J.*, vol. 4, no. 5, pp. 1536–1541, Oct. 2012, doi: 10.1109/JPHOT.2012.2211342.

[46] L. Liu, Z. Han, and S. He, "Novel surface plasmon waveguide for high integration," *Opt. Exp.*, vol. 13, no. 17, p. 6645, 2005, doi: 10.1364/opex.13.006645.

[47] G. Veronis and S. Fan, "Guided subwavelength plasmonic mode supported by a slot in a thin metal film," *Opt. Lett.*, vol. 30, no. 24, p. 3359, Dec. 2005, doi: 10.1364/ol.30.003359.

[48] M. Heydari, A. Habibzadeh-Sharif, and F. Jabbarzadeh, "Design of a compact refractive-index sensor based on surface plasmon polariton slot waveguide," *Photon. Nanostruct. Fundam. Appl.*, vol. 38, Feb. 2020, Art. no. 100755, doi: 10.1016/j.photonics.2019.100755.

[49] R. Ding et al., "Low-loss asymmetric strip-loaded slot waveguides in silicon-on-insulator," *Appl. Phys. Lett.*, vol. 98, no. 23, Jun. 2011, Art. no. 233303, doi: 10.1063/1.3597798.

[50] H. Zhang et al., "CMOS-compatible fabrication of silicon-based sub-100-nm slot waveguide with efficient channel-slot coupler," *IEEE Photon. Technol. Lett.*, vol. 24, no. 1, pp. 10–12, Jan. 2012, doi: 10.1109/LPT.2011.2171936.

[51] M. Hiltunen, E. Heinonen, J. Hiltunen, J. Puustinen, J. Lappalainen, and P. Karioja, "Nanoimprint fabrication of slot waveguides," *IEEE Photon. J.*, vol. 5, no. 2, Apr. 2013, Art. no. 2200808, doi: 10.1109/JPHOT.2013.2251876.

[52] Z. Han, A. Y. Elezzabi, and V. Van, "Experimental realization of subwavelength plasmonic slot waveguides on a silicon platform," *Opt. Lett.*, vol. 35, no. 4, p. 502, Feb. 2010, doi: 10.1364/ol.35.000502.

[53] B. Lau, M. A. Swillam, and A. S. Helmy, "Hybrid orthogonal junctions: Wideband plasmonic slot-silicon waveguide couplers," *Opt. Exp.*, vol. 18, no. 26, p. 27048, Dec. 2010, doi: 10.1364/oe.18.027048.

[54] T. Alasaarela et al., "Reduced propagation loss in silicon strip and slot waveguides coated by atomic layer deposition," *Opt. Exp.*, vol. 19, no. 12, p. 11529, Jun. 2011, doi: 10.1364/oe.19.011529.

[55] A. Säynätjoki et al., "Low-loss silicon slot waveguides and couplers fabricated with optical lithography and atomic layer deposition," *Opt. Exp.*, vol. 19, no. 27, p. 26275, Dec. 2011, doi: 10.1364/oe.19.026275.

[56] H. Sun, A. Chen, D. Abeysinghe, A. Szep, and R. S. Kim, "Reduction of scattering loss of silicon slot waveguides by RCA smoothing," *Opt. Lett.*, vol. 37, no. 1, p. 13, Jan. 2012, doi: 10.1364/ol.37.000013.

[57] R. M. Pafchek, J. Li, R. S. Tummidi, and T. L. Koch, "Low loss Si–SiO_2–Si 8-nm slot waveguides," *IEEE Photon. Technol. Lett.*, vol. 21, no. 6, pp. 353–355, Mar. 2009, doi: 10.1109/LPT.2008.2011651.

[58] G. M. Hale and M. R. Querry, "Optical constants of water in the 200-nm to 200-μm wavelength region," *Appl. Opt.*, vol. 12, no. 3, p. 555, Mar. 1973, doi: 10.1364/ao.12.000555.

[59] C. A. Barrios, "Optical slot-waveguide based biochemical sensors," *Sensors*, vol. 9, no. 6, pp. 4751–4765, Jun. 2009, doi: 10.3390/s90604751.

[60] C. A. Barrios, "Integrated microring resonator sensor arrays for labs-on-chips," *Anal. Bioanal. Chem.*, vol. 403, no. 6, pp. 1467–1475, Jun. 2012, doi: 10.1007/s00216-012-5937-3.

[61] C. A. Barrios et al., "Slot-waveguide biochemical sensor," *Opt. Lett.*, vol. 32, no. 21, p. 3080, Nov. 2007, doi: 10.1364/ol.32.003080.

[62] C. A. Barrios et al., "Label-free optical biosensing with slot-waveguides," *Opt. Lett.*, vol. 33, no. 7, p. 708, Apr. 2008, doi: 10.1364/ol.33.000708.

[63] T. Claes, J. G. Molera, K. De Vos, E. Schacht, R. Baets, and P. Bienstman, "Label-free biosensing with a slot-waveguide-based ring resonator in silicon on insulator," *IEEE Photon. J.*, vol. 1, no. 3, pp. 197–204, Sep. 2009, doi: 10.1109/JPHOT.2009.2031596.

[64] C. F. Carlborg et al., "A packaged optical slot-waveguide ring resonator sensor array for multiplex label-free assays in labs-on-chips," *Lab Chip*, vol. 10, no. 3, pp. 281–290, 2010, doi: 10.1039/b914183a.

[65] T. Taniguchi et al., "Detection of antibody-antigen reaction by silicon nitride slot-ring biosensors using protein G," *Opt. Commun.*, vol. 365, pp. 16–23, Apr. 2016, doi: 10.1016/j.optcom.2015.11.068.

[66] P. Steglich et al., "Hybrid-waveguide ring resonator for biochemical sensing," *IEEE Sensors J.*, vol. 17, no. 15, pp. 4781–4790, Aug. 2017, doi: 10.1109/JSEN.2017.2710318.

[67] S. Shawky, A. H. A. El-Malek, A. Allam, and H. M. H. Shalaby, "A new SOI sensor design for detecting cancer using hybrid waveguide with higher sensitivity than both strip and slot waveguides," *Opt. Quantum Electron.*, vol. 56, no. 3, p. 483, Mar. 2024, doi: 10.1007/s11082-023-06082-z.

[68] T. Dar, J. Homola, B. M. A. Rahman, and M. Rajarajan, "Label-free slot-waveguide biosensor for the detection of DNA hybridization," *Appl. Opt.*, vol. 51, no. 34, p. 8195, Nov. 2012, doi: 10.1364/AO.51.008195.

[69] G. Yuan, L. Gao, Y. Chen, X. Liu, J. Wang, and Z. Wang, "Improvement of optical sensing performances of a double-slot-waveguide-based ring resonator sensor on silicon-on-insulator platform," *Optik*, vol. 125, no. 2, pp. 850–854, Jan. 2014, doi: 10.1016/j.ijleo.2013.07.088.

[70] B. Shi, X. Chen, Y. Cai, S. Zhang, T. Wang, and Y. Wang, "Compact slot microring resonator for sensitive and label-free optical sensing," *Sensors*, vol. 22, no. 17, p. 6467, Aug. 2022, doi: 10.3390/s22176467.

[71] P. J. Bock et al., "Subwavelength grating periodic structures in silicon-on-insulator: A new type of microphotonic waveguide," *Opt. Exp.*, vol. 18, no. 19, p. 20251, Sep. 2010, doi: 10.1364/oe.18.020251.

[72] J. Flueckiger et al., "Sub-wavelength grating for enhanced ring resonator biosensor," *Opt. Exp.*, vol. 24, no. 14, p. 15672, 2016, doi: 10.1364/OE.24.015672.

[73] E. Luan et al., "Enhanced sensitivity of subwavelength multibox waveguide microring resonator label-free biosensors," *IEEE J. Sel. Topics Quantum Electron.*, vol. 25, no. 3, pp. 1–11, May 2019, doi: 10.1109/JSTQE.2018.2821842.

[74] D. P. Campbell, "Interferometric biosensors," in *Principles of Bacterial Detection: Biosensors, Recognition Receptors and Microsystems*, M. Zourob, S. Elwary, and A. Turner, Eds., New York, NY, USA: Springer, 2008, pp. 169–211, doi: 10.1007/978-0-387-75113-9_9.

[75] V. M. N. Passaro, F. Dell'Olio, C. Ciminelli, and M. N. Armenise, "Efficient chemical sensing by coupled slot SOI waveguides," *Sensors*, vol. 9, no. 2, pp. 1012–1032, Feb. 2009, doi: 10.3390/s90201012.

[76] Q. Liu et al., "Highly sensitive Mach–Zehnder interferometer biosensor based on silicon nitride slot waveguide," *Sens. Actuators B, Chem.*, vol. 188, pp. 681–688, Nov. 2013, doi: 10.1016/j.snb.2013.07.053.

[77] X. Sun, D. Dai, L. Thylén, and L. Wosinski, "High-sensitivity liquid refractive-index sensor based on a Mach–Zehnder interferometer with a double-slot hybrid plasmonic waveguide," *Opt. Exp.*, vol. 23, no. 20, p. 25688, Oct. 2015, doi: 10.1364/oe.23.025688.

[78] X. Ma, K. Chen, J. Wu, and L. Wang, "Low-cost and highly sensitive liquid refractive index sensor based on polymer horizontal slot waveguide," *Photonic Sensors*, vol. 10, no. 1, pp. 7–15, Mar. 2020, doi: 10.1007/s13320-019-0560-y.

[79] S. P. Kumaar and A. Sivasubramanian, "Analysis of BCB and SU 8 photonic waveguide in MZI architecture for point-of-care devices," *Sensors Int.*, vol. 4, Jan. 2023, Art. no. 100207, doi: 10.1016/j.sintl.2022.100207.

[80] S. P. Kumaar and A. Sivasubramanian, "Design of a high-sensitivity polymer double-slot waveguide sensor for point-of-care biomedical applications," *Sensors Int.*, vol. 5, Jan. 2024, Art. no. 100255, doi: 10.1016/j.sintl.2023.100255.

[81] M. Hiltunen et al., "Polymeric slot waveguide interferometer for sensor applications," *Opt. Exp.*, vol. 22, no. 6, p. 7229, Mar. 2014, doi: 10.1364/oe.22.007229.

[82] D. Gowdhami, V. R. Balaji, M. Murugan, S. Robinson, and G. Hegde, "Photonic crystal based biosensors: An overview," *ISSS J. Micro Smart Syst.*, vol. 11, no. 1, pp. 147–167, Jun. 2022, doi: 10.1007/s41683-022-00092-x.

[83] A. Di Falco, L. O'Faolain, and T. F. Krauss, "Chemical sensing in slotted photonic crystal heterostructure cavities," *Appl. Phys. Lett.*, vol. 94, no. 6, Feb. 2009, Art. no. 063503, doi: 10.1063/1.3079671.

[84] J. Jágerská, H. Zhang, Z. Diao, N. L. Thomas, and R. Houdré, "Refractive index sensing with an air-slot photonic crystal nanocavity," *Opt. Lett.*, vol. 35, no. 15, p. 2523, Aug. 2010, doi: 10.1364/ol.35.002523.

[85] M. G. Scullion, A. Di Falco, and T. F. Krauss, "Slotted photonic crystal cavities with integrated microfluidics for biosensing applications," *Biosensors Bioelectron.*, vol. 27, no. 1, pp. 101–105, Sep. 2011, doi: 10.1016/j.bios.2011.06.023.

[86] S. H. Mirsadeghi, E. Schelew, and J. F. Young, "Photonic crystal slot-microcavity circuit implemented in silicon-on-insulator: High Q operation in solvent without undercutting," *Appl. Phys. Lett.*, vol. 102, no. 13, Apr. 2013, Art. no. 131115, doi: 10.1063/1.4799963.

[87] L. Huang, H. Tian, J. Zhou, Q. Liu, P. Zhang, and Y. Ji, "Label-free optical sensor by designing a high-Q photonic crystal ring–slot structure," *Opt. Commun.*, vol. 335, pp. 73–77, Jan. 2015, doi: 10.1016/j.optcom.2014.09.014.

[88] B. Wang, M. A. Dündar, R. Nötzel, F. Karouta, S. He, and R. W. van der Heijden, "Photonic crystal slot nanobeam slow light waveguides for refractive index sensing," *Appl. Phys. Lett.*, vol. 97, no. 15, Oct. 2010, Art. no. 151105, doi: 10.1063/1.3497296.

[89] P. Xu, K. Yao, J. Zheng, X. Guan, and Y. Shi, "Slotted photonic crystal nanobeam cavity with parabolic modulated width stack for refractive index sensing," *Opt. Exp.*, vol. 21, no. 22, p. 26908, Nov. 2013, doi: 10.1364/oe.21.026908.

[90] D. Yang et al., "High sensitivity and high Q-factor nanoslotted parallel quadrabeam photonic crystal cavity for real-time and label-free sensing," *Appl. Phys. Lett.*, vol. 105, no. 6, Aug. 2014, Art. no. 063118, doi: 10.1063/1.4867254.

[91] J. Zhou, H. Tian, D. Yang, Q. Liu, L. Huang, and Y. Ji, "Refractive index sensing utilizing parallel tapered nano-slotted photonic crystal nano-beam cavities," *J. Opt. Soc. Amer. B, Opt. Phys.*, vol. 31, no. 8, p. 1746, Aug. 2014, doi: 10.1364/josab.31.001746.

[92] F. Sun, J. Zhou, L. Huang, Z. Fu, and H. Tian, "High quality factor and high sensitivity photonic crystal rectangular holes slot nanobeam cavity with parabolic modulated lattice constant for refractive index sensing," *Opt. Commun.*, vol. 399, pp. 56–61, Sep. 2017, doi: 10.1016/j.optcom.2017.04.016.

[93] C.-S. Deng, M.-J. Li, J. Peng, W.-L. Liu, and J.-X. Zhong, "Simultaneously high-Q and high-sensitivity slotted photonic crystal nanofiber cavity for complex refractive index sensing," *J. Opt. Soc. Amer. B, Opt. Phys.*, vol. 34, no. 8, p. 1624, Aug. 2017, doi: 10.1364/josab.34.001624.

[94] P. Xu, J. Zheng, J. Zhou, Y. Chen, C. Zou, and A. Majumdar, "Multi-slot photonic crystal cavities for high-sensitivity refractive index sensing," *Opt. Exp.*, vol. 27, no. 3, p. 3609, Feb. 2019, doi: 10.1364/oe.27.003609.

[95] A. Yariv and P. Yeh, *Photonics: Optical Electronics in Modern Communication*. New York, NY, USA: Oxford Univ. Press, 2007, p. 559.

[96] P. Prabhathan, V. M. Murukeshan, Z. Jing, and P. V. Ramana, "Compact SOI nanowire refractive index sensor using phase shifted Bragg grating," *Opt. Exp.*, vol. 17, no. 17, p. 15330, 2009, doi: 10.1364/oe.17.015330.

[97] H.-C. Kim, K. Ikeda, and Y. Fainman, "Tunable transmission resonant filter and modulator with vertical gratings," *J. Lightw. Technol.*, vol. 25, no. 5, pp. 1147–1151, May 2007, doi: 10.1109/jlt.2007.893922.

[98] X. Wang, W. Shi, H. Yun, S. Grist, N. A. Jaeger, and L. Chrostowski, "Narrow-band waveguide Bragg gratings on SOI wafers with CMOS-compatible fabrication process," *Opt. Exp.*, vol. 20, no. 14, pp. 15547–15558, 2012, doi: 10.1364/OE.20.015547.

[99] A. S. Jugessur, M. Yagnyukova, J. Dou, and J. S. Aitchison, "Bragg-grating air-slot optical waveguide for label-free sensing," *Proc. SPIE*, vol. 8231, Feb. 2012, Art. no. 82310N, doi: 10.1117/12.908562.

[100] X. Wang et al., "A silicon photonic biosensor using phase-shifted Bragg gratings in slot waveguide," *J. Biophotonics*, vol. 6, no. 10, pp. 821–828, Oct. 2013, doi: 10.1002/jbio.201300012.

[101] E. Luan, H. Yun, M. Ma, D. M. Ratner, K. C. Cheung, and L. Chrostowski, "Label-free biosensing with a multi-box sub-wavelength phase-shifted Bragg grating waveguide," *Biomed. Opt. Exp.*, vol. 10, no. 9, p. 4825, 2019.

[102] S. Heinsalu, Y. Isogai, Y. Matsushima, H. Ishikawa, and K. Utaka, "Record-high sensitivity compact multi-slot sub-wavelength Bragg grating refractive index sensor on SOI platform," *Opt. Exp.*, vol. 28, no. 19, p. 28126, Sep. 2020, doi: 10.1364/oe.402672.

[103] X. Wang and C. K. Madsen, "Highly sensitive compact refractive index sensor based on phase-shifted sidewall Bragg gratings in slot waveguide," *Appl. Opt.*, vol. 53, no. 1, p. 96, Jan. 2014, doi: 10.1364/ao.53.000096.

[104] S. Sahu, J. Ali, and G. Singh, "Refractive index biosensor using sidewall gratings in dual-slot waveguide," *Opt. Commun.*, vol. 402, pp. 408–412, Nov. 2017, doi: 10.1016/j.optcom.2017.06.051.

[105] Q. Liu, J. S. Kee, and M. K. Park, "A refractive index sensor design based on grating-assisted coupling between a strip waveguide and a slot waveguide," *Opt. Exp.*, vol. 21, no. 5, p. 5897, Mar. 2013, doi: 10.1364/oe.21.005897.

[106] L. Singh, S. Jain, and M. Kumar, "Nanophotonic device based on Fano resonance in engineered slot waveguide for optical detection of viral infections," *IEEE Sensors J.*, vol. 21, no. 3, pp. 2805–2812, Feb. 2021, doi: 10.1109/JSEN.2020.3023146.

[107] C. Y. Zhao, L. Zhang, and C. M. Zhang, "Compact SOI optimized slot microring coupled phase-shifted Bragg grating resonator for sensing," *Opt. Commun.*, vol. 414, pp. 212–216, May 2018, doi: 10.1016/j.optcom.2018.01.010.

[108] N. Wu and L. Xia, "High-Q and high-sensitivity multi-hole slot microring resonator and its sensing performance," *Phys. Scripta*, vol. 94, no. 11, Nov. 2019, Art. no. 115512, doi: 10.1088/1402-4896/ab3266.

[109] H. Gu et al., "Compact inner-wall grating slot microring resonator for label-free sensing," *Sensors*, vol. 19, no. 22, p. 5038, Nov. 2019, doi: 10.3390/s19225038.

[110] F. Dell'Olio and V. M. Passaro, "Optical sensing by optimized silicon slot waveguides," *Opt. Exp.*, vol. 15, no. 8, p. 4977, 2007, doi: 10.1364/OE.15.004977.

[111] P. Bettotti, A. Pitanti, E. Rigo, F. De Leonardis, V. M. N. Passaro, and L. Pavesi, "Modeling of slot waveguide sensors based on polymeric materials," *Sensors*, vol. 11, no. 8, pp. 7327–7340, Jul. 2011, doi: 10.3390/s110807327.

[112] L. Ahmadi, J. Tervo, J. Saarinen, and S. Honkanen, "Enhanced sensitivity in polymer slot waveguides by atomic layer deposited bilayer coatings," *Appl. Opt.*, vol. 52, no. 33, p. 8089, Nov. 2013, doi: 10.1364/ao.52.008089.

[113] C. Viphavakit, M. Komodromos, C. Themistos, W. S. Mohammed, K. Kalli, and B. M. Azizur Rahman, "Optimization of a horizontal slot waveguide biosensor to detect DNA hybridization," *Appl. Opt.*, vol. 54, no. 15, p. 4881, May 2015, doi: 10.1364/AO.54.004881.

[114] C. Pan and B. M. A. Rahman, "High-sensitivity polarization-independent biochemical sensor based on Silicon-on-Insulator cross-slot waveguide," *IEEE J. Sel. Topics Quantum Electron.*, vol. 23, no. 2, pp. 64–71, Mar. 2017, doi: 10.1109/JSTQE.2016.2594094.

[115] M. A. Butt, S. N. Khonina, and N. L. Kazanskiy, "A highly sensitive design of subwavelength grating double-slot waveguide microring resonator," *Laser Phys. Lett.*, vol. 17, no. 7, Jul. 2020, Art. no. 076201, doi: 10.1088/1612-202x/ab8faa.

[116] R. Bernini, N. Cennamo, A. Minardo, and L. Zeni, "Planar waveguides for fluorescence-based biosensing: Optimization and analysis," *IEEE Sensors J.*, vol. 6, no. 5, pp. 1218–1226, Oct. 2006, doi: 10.1109/JSEN.2006.881408.

[117] C. A. Barrios, "Ultrasensitive nanomechanical photonic sensor based on horizontal slot-waveguide resonator," *IEEE Photon. Technol. Lett.*, vol. 18, no. 22, pp. 2419–2421, Nov. 2006.

[118] J. Langer et al., "Present and future of surface-enhanced Raman scattering," *ACS Nano*, vol. 14, no. 1, pp. 28–117, Jan. 2020, doi: 10.1021/acsnano.9b04224.

[119] P. Wang and B. L. Miller, "Waveguide-enhanced Raman spectroscopy (WERS): An emerging chip-based tool for chemical and biological sensing," *Sensors*, vol. 22, no. 23, p. 9058, Nov. 2022, doi: 10.3390/s22239058.

[120] A. Dhakal et al., "Efficiency of evanescent excitation and collection of spontaneous Raman scattering near high index contrast channel waveguides," *Opt. Exp.*, vol. 23, no. 21, p. 27391, Oct. 2015, doi: 10.1364/oe.23.027391.

[121] Z. Liu et al., "Ultra-sensitive slot-waveguide-enhanced Raman spectroscopy for aqueous solutions of non-polar compounds using a functionalized silicon nitride photonic integrated circuit," *Opt. Lett.*, vol. 46, no. 5, p. 1153, Mar. 2021, doi: 10.1364/ol.416464.

[122] N. Turk et al., "Waveguide-based surface-enhanced Raman spectroscopy detection of protease activity using non-natural aromatic amino acids," *Biomed. Opt. Exp.*, vol. 11, no. 8, p. 4800, Aug. 2020, doi: 10.1364/boe.398038.

[123] J. Wu et al., "On-chip optical gas sensors based on group-IV materials," *ACS Photon.*, vol. 7, no. 11, pp. 2923–2940, Nov. 2020, doi: 10.1021/acsphotonics.0c00976.

[124] J. T. Robinson, L. Chen, and M. Lipson, "On-chip gas detection in silicon optical microcavities," *Opt. Exp.*, vol. 16, no. 6, p. 4296, Mar. 2008, doi: 10.1364/oe.16.004296.

[125] N. A. Yebo, P. Lommens, Z. Hens, and R. Baets, "An integrated optic ethanol vapor sensor based on a silicon-on-insulator microring resonator coated with a porous ZnO film," *Opt. Exp.*, vol. 18, no. 11, p. 11859, May 2010, doi: 10.1364/oe.18.011859.

[126] W.-C. Lai, S. Chakravarty, X. Wang, C. Lin, and R. T. Chen, "On-chip methane sensing by near-IR absorption signatures in a photonic crystal slot waveguide," *Opt. Lett.*, vol. 36, no. 6, p. 984, Mar. 2011, doi: 10.1364/ol.36.000984.

[127] W.-C. Lai, S. Chakravarty, X. Wang, C. Lin, and R. T. Chen, "Photonic crystal slot waveguide absorption spectrometer for on-chip near-infrared spectroscopy of xylene in water," *Appl. Phys. Lett.*, vol. 98, no. 2, Jan. 2011, Art. no. 023304, doi: 10.1063/1.3531560.

[128] C. Blin et al., "Surface-sensitive diamond photonic crystals for high-performance gas detection," *Opt. Lett.*, vol. 41, no. 18, p. 4360, Sep. 2016, doi: 10.1364/ol.41.004360.

[129] H. D. Yallew et al., "Sub-ppm methane detection with mid-infrared slot waveguides," *ACS Photon.*, vol. 10, no. 12, pp. 4282–4289, Dec. 2023, doi: 10.1021/acsphotonics.3c01085.

[130] Y. Huang, S. K. Kalyoncu, Q. Zhao, R. Torun, and O. Boyraz, "Silicon-on-sapphire waveguides design for mid-IR evanescent field absorption gas sensors," *Opt. Commun.*, vol. 313, pp. 186–194, Feb. 2014, doi: 10.1016/j.optcom.2013.10.022.

[131] B. Kumari, A. Barh, R. K. Varshney, and B. P. Pal, "Silicon-on-nitride slot waveguide: A promising platform as mid-IR trace gas sensor," *Sens. Actuators B, Chem.*, vol. 236, pp. 759–764, Nov. 2016, doi: 10.1016/j.snb.2016.06.060.

[132] Z. Cheng and K. Goda, "Design of waveguide-integrated graphene devices for photonic gas sensing," *Nanotechnology*, vol. 27, no. 50, Dec. 2016, Art. no. 505206, doi: 10.1088/0957-4484/27/50/505206.

[133] D. Zhang et al., "Ultra-high-enhancement-factor integrated long-wave infrared gas sensor based on the tapered sub-wavelength grating slot waveguide," *Results Phys.*, vol. 48, May 2023, Art. no. 106442, doi: 10.1016/j.rinp.2023.106442.

[134] J. Liao et al., "On-chip long-wave infrared gas sensor based on subwavelength grating waveguide," *J. Nanophotonics*, vol. 17, no. 3, Sep. 2023, Art. no. 036011, doi: 10.1117/1.jnp.17.036011.

[135] Y. Qiao, J. Tao, J. Qiu, X. Hong, and J. Wu, "Sensitive and ultra-small sample volume gas sensor based on a sealed slot waveguide," *Appl. Opt.*, vol. 58, no. 17, p. 4708, Jun. 2019, doi: 10.1364/ao.58.004708.

[136] G. Xu et al., "Design and analysis of slow-light bloch slot waveguides for on-chip gas sensing," *J. Opt. Soc. Amer. B, Opt. Phys.*, vol. 37, no. 2, p. 257, Feb. 2020, doi: 10.1364/josab.380251.

[137] A. la Grasta et al., "Silicon-on-Insulator microphotonic resonators for label-free biosensing: An experiment-based comparison between the different configurations," *IEEE Sensors J.*, vol. 24, no. 14, pp. 22351–22358, Jul. 2024, doi: 10.1109/JSEN.2024.3406945.

Open Access funding provided by 'Politecnico di Bari' within the CRUI CARE Agreement